# Origin, distributions, and environmental significance of ubiquitous humic-like fluorophores in Antarctic lakes and streams

Kida, Morimaru ; Kojima, Taichi ; Tanabe, Yukiko ; Hayashi, Kentaro ; Kudoh, Sakae ; Maie, Nagamitsu ; Fujitake, Nobuhide

(Citation)
Water Research,163:114901

(Issue Date)
2019-10-15

(Resource Type)
journal article

(Version)
Accepted Manuscript

# Origin, distributions, and environmental significance of ubiquitous humic-like fluorophores in Antarctic lakes and streams

Journal: Water Research

**Morimaru Kida[1†‡*], Taichi Kojima[1], Yukiko Tanabe[2, 3], Kentaro Hayashi[4], Sakae Kudoh[2, 3], Nagamitsu Maie[5], Nobuhide Fujitake[1]**

[1] Graduate School of Agricultural Science, Kobe University, 1-1 Rokkodai, Nada, Kobe, Hyogo 657-8501, Japan

[2] National Institute of Polar Research, Research Organization of Information and Systems, 10-3 Midori-cho, Tachikawa, Tokyo 190-8518, Japan

[3] Department of Polar Science, SOKENDAI (The Graduate University for Advanced Studies), 10-3 Midori-cho, Tachikawa, Tokyo 190-8518, Japan

[4] Institute for Agro-Environmental Sciences, NARO, 3-1-3 Kannondai, Tsukuba, Ibaraki 305-8604, Japan

[5] School of Veterinary Medicine, Kitasato University, Towada, Aomori 034-8628, Japan

† Research Fellow of Japan Society for the Promotion of Science

19 ‡ Present address: Research Group for Marine Geochemistry (ICBM-MPI Bridging Group), Carl
20 von Ossietzky University of Oldenburg, Institute for Chemistry and Biology of the Marine
21 Environment (ICBM), Carl-von-Ossietzky-Str. 9-11, 26129 Oldenburg, Germany
22
23 * corresponding author
24 morimaru.kida@people.kobe-u.ac.jp
25 ORCID ID: 0000-0002-9908-2012 (M.K.), 0000-0002-2936-9544 (K.H.)
26

**Abstract**

This study characterized dissolved organic matter (DOM) obtained from 47 lakes and 2 streams on ice-free areas at Lützow-Holm Bay and Amundsen Bay in East Antarctica ($n$ = 74), where few biogeochemical studies have been historically conducted. Samples were analyzed for basic water chemistry and by resin fractionation, UV-vis spectroscopy, and excitation emission matrix spectroscopy combined with parallel factor analysis (EEM-PARAFAC). Salinity of the samples ranged very broadly from fresh to hypersaline as a result of evaporative concentration. There was a clear positive correlation between log-salinity and the spectral slopes of DOM ($S_{275–295}$), an indicator of photodegradation. Thus, we interpreted the correlation as a progression of photodegradation by prolonged water retention time. Of the identified seven PARAFAC components, three ubiquitous humic-like components decreased as photodegradation progressed, while a photorefractory UVC humic-like component increased its relative abundance. A non-humic component, traditionally defined as Peak N, did not show a trend depending on photodegradation, and its level was high in nutrient-rich lakes, presumably due to high in-situ production. We found robust correlations between the relative abundance of the ubiquitous humic-like components and that of the Peak N component in the bulk DOM irrespective of water types or ice-free areas. We proposed there were common processes that generated the ubiquitous humic-like components from the Peak N component in the Lützow-Holm Bay and Amundsen Bay lakes and streams, such as bacterial processing of primary

45 production-derived DOM and photochemical transformation of microbial DOM.

46

47 **Keywords**

48 autochthonous; DOM; fluorescence; microbial process; PARAFAC; photodegradation

49

50

## 1. Introduction

Dissolved organic matter (DOM) is a highly heterogeneous collection of hundreds of thousands of organic compounds that collectively play an essential role in key ecosystem processes (Zark et al., 2017). DOM ubiquitously exists in water and comprises a similar mass of carbon as atmospheric $CO_2$ or the global biomass (Hedges et al., 1997). DOM is involved in various biogeochemical processes, such as light attenuation, metal complexation, pH buffering, and influencing microbial metabolism (Findlay and Sinsabaugh, 2003), and is one of the most important components on Earth that influences the health of ecosystems.

The chemical composition and functionality of DOM is strongly influenced by the original source and ecosystem activities (Roth et al., 2014). DOM in streams and peatland rivers often contains a high proportion of terrestrial lignin-derived materials, while that in large lakes and oceans usually contains a high proportion of microbial-derived matter. Aside from the ecosystem-specificity of DOM, molecularly and photochemically indistinguishable ubiquitous components of DOM have been recently identified in samples from diverse environments (Murphy et al., 2018; Zark and Dittmar, 2018). These findings imply that there are some common mechanisms that produce these ubiquitous components in DOM, such as either biotic or abiotic pathways that lead to the production of ubiquitous, recalcitrant components of DOM that persist in the environment. Unraveling the underlying mechanisms of the generation of these components is one of the key questions in

69 understanding transformation and long-term turnover of DOM (Murphy et al., 2018; Zark and
70 Dittmar, 2018).

71 In ice-free areas of continental Antarctica, where no vascular plants are present, DOM is
72 originated dominantly from in-situ biological activity (both benthic and planktonic phototrophs) in
73 water and phototrophs (mosses, algae, lichens, cyanobacteria) in the catchments (Matsumoto, 1989;
74 McKnight et al., 1994, 1991). Furthermore, because lakes are isolated from each other with
75 independent water catchment areas by impermeable bedrocks, they function as closed hydrologic
76 systems. The simplicity of the organic matter sources and the lack of the connection with other
77 hydrologic systems limit the number of environmental factors that would otherwise make it difficult
78 to elucidate processes responsible for DOM transformations. Due to the simplicity of the sources, the
79 chemical characteristics of Antarctic lake DOM have been considered to vary little among Antarctic
80 lakes (Aiken et al., 1996; McKnight et al., 1991). However, past studies were exclusively conducted
81 in the McMurdo Dry Valleys of East Antarctica (Matsumoto, 1989; McKnight et al., 1994, 1991),
82 and very few biogeochemical studies on DOM chemistry have been conducted in other regions in
83 Antarctica (Farzadnia et al., 2017).

84 Here, we report an extensive study conducted in 47 lakes and 2 streams in 6 ice-free areas
85 at Lützow-Holm Bay (East Dronning Maud Land) and Amundsen Bay (Enderby Land) in East
86 Antarctica. This was by far the largest and most diverse dataset that has been historically obtained

from Antarctic lakes. The overall goal of this study was to use spectroscopic techniques to evaluate the potential sources and sinks of DOM in these lakes and streams. Spectroscopic techniques that were used in this study, such as UV-vis spectroscopy and excitation-emission matrix spectroscopy (EEM), have been successful in studying concentrations, compositions, and dynamics of chromophoric (CDOM) and fluorescent DOM (FDOM) in aquatic systems including Antarctic lakes (Cawley et al., 2016, 2013; McKnight et al., 1994). We hypothesized that DOM in the Antarctic lakes and streams has much larger compositional diversity than has been considered and such diversity is mostly introduced by external factors such as photodegradation because the simplicity of the sources would reduce the original DOM heterogeneity. Studying the geochemistry of diverse microbially-dominated lake systems should lead to a better understanding of lower latitude aquatic systems as well, where several end-members form a continuum of DOM characteristics.

## 2. Materials and Methods

### 2.1. Study area

The main sampling campaign was conducted during the austral summer during December 2016 and February 2017 in ice-free areas along Sôya Coast (Lützow-Holm Bay, East Dronning Maud Land), located in the southern area of Syowa Station (Japan's base) (Fig. S1). In Sôya Coast, there are several ice-free areas, including Skarvsnes, Langhovde, Skallen, Breidvågnipa, and Rundvågshetta,

105 where hundreds of lakes of various sizes and water chemistry exist (Imura et al., 2003; Kimura et al.,
106 2010; Kudoh and Tanabe, 2014). These ice-free areas were created during the last 7,000 years under
107 the glacier retreat and iso-static uplifts that occurred after the Last Glacial Maximum (Kudoh and
108 Tanabe, 2014). Almost no lakes have any in- or out flows, and they are fed by melt water from
109 adjacent glaciers and/or snow and ice in their catchments. The lakes have been isolated from each
110 other with independent water catchment areas, and they function as closed hydrologic systems. A 1–
111 2 m thick ice cover usually develops on all lakes during March-December (or January) (Imura et al.,
112 2003). Additional water sampling was conducted in an ice-free area at the foot of Mt. Riiser-Larsen,
113 Amundsen Bay, West Enderby Land. A large number of Adélie penguins (*Pygoscelis adeliae*) (>
114 1800 breeding pairs) and emperor penguins (*Aptenodytes forsteri*) have been reported in this region
115 (Takahashi et al., 2000), which would influence the lake water chemistry and biology.

116 Water chemistry of the lakes in Sôya Coast is very diverse despite sharing the same
117 climate, suggesting that it would induce the diversity in lake water DOM as well. For example,
118 salinity ranges from completely fresh to saline to hypersaline, i.e., more than seven times the salinity
119 of seawater (Matsumoto, 1989). Although most of the saline lakes are considered to have been
120 generated via the evaporative concentration of lake water under dry conditions, others are marine
121 relict lakes, which were in the shallow coastal sea and formed after the iso-static uplift of the present
122 lake shores. The evapo-concentration of Sôya Coast lakes occurs at variable rates reflecting the

123 balance between evaporation and freshwater inputs. When freshwater inputs dominate, even marine
124 relict lakes can have zero salinity after a long period (see Table 1). In contrast to salinity,
125 concentrations of essential nutrients for phototroph growth, such as nitrate and phosphate, are quite
126 low in most of the lakes, rendering them oligotrophic. Waters in proglacial lakes (lakes located in
127 front of or close to a glacier) exhibit ultra-oligotrophic freshwater conditions. They typically contain
128 inorganic particles derived from glacial deposits; thus, the water transparency is low despite the
129 ultra-oligotrophic state. Proglacial lakes directly attached to the glacier terminal tend to have
130 permanent ice covers, which can develop up to 4-m thick in winter. Geological, limnological, and
131 ecological characteristics of many of the sampled lakes have been described and reviewed elsewhere
132 (Imura et al., 2003; Kimura et al., 2010; Kudoh and Tanabe, 2014)
133
134 **2.2. Water sampling and handling**
135 Water samples were collected at the deepest point ($n$ = 19) or shore ($n$ = 28) of 47 lakes in the
136 ice-free areas at Lützow-Holm Bay and Amundsen Bay (Fig. S1). Two streams (Yukidori and
137 Yatsude Valleys in Langhovde, $n$ = 16) were additionally sampled for comparison to lakes. The
138 sampling locations, limnological characteristics, and basic optical and chemical properties of DOM
139 for each lake are presented in Table 1, while those for streams are presented in Table S1. Stream
140 samples were collected at approximately regular intervals from the beginning (glacial melt) to the

141 end (before the outlet to the sea) of each stream. At the streams and lake shores, samples were
142 directly collected into 550-mL volume polyethylene terephthalate bottles after rinsing more than
143 three times with the collected water. The pH, salinity (*S*), and water temperature were recorded in
144 situ using portable water quality meters (LAQUA series, Horiba, Kyoto, Japan). At the deepest point
145 of the lakes (checked using a portable sonar depth meter, PS-7, Hondex, Aichi, Japan), after the
146 confirmation of uniformity in water properties by a multi-water quality logger (YSI-6600V2, YSI
147 Inc., OH, USA) (Fig. S2), lake water was collected at mid-depth of the water column using a Teflon
148 cylindrical water sampler into the bottles. When water stratification was observed, water was
149 collected at several depths to capture changes in water chemistry (Figs. S2 i–l). At five lakes (Figs.
150 S2 b–d, p, and q), porewater was sampled from sediment cores that were collected using a gravity
151 corer with a transparent acrylic pipe (diameter 5 cm, length 50 cm) (Fig. S1e). After gently
152 aspirating water above the sediment cores (bottom water) using a glass pipet, porewater was
153 collected and stored in the dark.

154 The collected waters were filtered in field laboratories as soon as possible, usually within a
155 few hours after sampling. Fourteen samples collected in Skallen, Breidvågnipa, and Rundvågshetta
156 were filtered in the field laboratory in Skarvsnes 1–3 days after sampling because of a logistical
157 limitation. Samples collected in Amundsen Bay were filtered in a laboratory on the ice breaking ship
158 “Shirase” on the day of sampling. Samples for dissolved organic carbon (DOC), total dissolved

159 nitrogen (TDN), and optical analysis were filtered through pre-combusted (450°C, > 3 h) glass fiber
160 filters (nominal pore size 0.3 μm, GF-75, Advantec, Tokyo, Japan) into pre-combusted glass bottles.
161 A 50-mL aliquot of GF-75 filtered samples was stored in a plastic bottle and kept frozen (−20°C) for
162 inorganic nutrient analysis. The samples for DOC and TDN analysis were spiked with sodium azide
163 (final concentration of 0.02%) and hydrochloric acid (final concentration of 1%), respectively (Wako
164 Pure Chemical, Osaka, Japan), and stored for further analysis in Japan. Optical analysis was
165 performed immediately after filtration in the field laboratory in Skarvsnes or on Shirase.
166
167 **2.3. Water analysis**
168 UV-vis absorption spectra (240–600 nm) were measured using a UV-visible spectrophotometer
169 (GENESYS 10S UV-Vis, Thermo Fisher Scientific, Tokyo, Japan) with a 5-cm path length,
170 acid-cleaned, quartz cuvette at ambient temperature. Some samples with a high optical density were
171 measured with a 1-cm path length cuvette. Measurements were baseline-corrected using ultrapure
172 water (Wako Pure Chemical, Osaka, Japan). Overestimation of absorbance by scatter was evident in
173 some samples, which was most likely due to clay-sized inorganic particles that passed through the
174 GF-75 filter. Such samples were mostly from proglacial lakes, where lake water was turbid from silt
175 and clay-sized particles fed by glaciers (Table 1). Absorbance data in this paper are expressed as
176 Napierian absorption coefficients ($a_\lambda$, $m^{-1}$). Absorption coefficients of DOM were calculated from

$a_\lambda = 2.303 A_\lambda / l$

where $A_\lambda$ is the absorbance at wavelength λ and $l$ is the cell path length in meters (Helms et al., 2008).

Fluorescence EEMs were collected with a spectrofluorometer (FluoroMax4, Horiba, Kyoto, Japan) equipped with a 150 W xenon arc lamp at room temperature using 5 nm excitation and emission slit widths, integration time of 0.25 s, excitation (Ex) range of 240–450 nm at 5 nm increments, and an emission (Em) range of 300–550 nm at 2 nm increments. A sharp peak of the xenon lamp emission (467 nm) and Raman peak (397 nm) were checked daily and corrected if they deviated > 0.5 nm from the desired values. The EEMs were corrected for all necessary steps to remove biases and normalized in Raman units (RU) (Murphy et al., 2018). Blank EEM (ultrapure water) used for blank subtraction and Raman normalization was measured daily.

In the laboratory in Japan, we measured DOC and TDN using a total organic carbon analyzer combined with a total nitrogen measuring unit (TOC-$L_{CPH}$, Shimadzu, Kyoto, Japan) as in Kida et al. (2019). Also, DOM in the samples was fractionated into hydrophobic (HPO) and hydrophilic DOM based on adsorption onto Supelite™ DAX-8 resin in quadruplicate according to Kida et al. (2019). DOM fractions retained on the DAX-8 resin (HPO) included hydrophobic acids (i.e., humic substances) and neutrals, which are too hydrophobic to be eluted by dilute alkali solution, such as less oxygenated humic substances, hydrocarbons, carbonyl compounds, and some

anthropogenic matter. The proportion of HPO in DOM (%HPO) was calculated by [HPO]/[DOM] × 100 on a carbon basis. The coefficient of variation of replicate %HPO determination measurements was < 17% (average ± one standard deviation SD, 4.9% ± 4.4%; Fig. S3b).

Dissolved inorganic nutrients ($PO_4^{3-}$, $NH_4^+$, $NO_2^-$, $NO_3^-$, and $SiO_3^{2-}$) were determined colorimetrically using an auto analyzer as previously reported (Tanabe et al., 2017). The limits of detection and quantitation were determined as the average plus 3 or 10 SD of the 10 × blank measurements, respectively. $NO_3^-$ concentrations were determined as the difference between ($NO_2^-$ + $NO_3^-$) concentrations minus $NO_2^-$ concentrations with or without a $NO_3^-$ reduction step. A dissolved organic nitrogen (DON) concentration was calculated as the difference between TDN and the sum of dissolved inorganic nitrogen concentrations. If any of the dissolved inorganic nitrogen concentrations were below the detection limit, a DON concentration was calculated as the difference between TDN and the sum of the rest of the detected dissolved inorganic nitrogen concentrations. The proportion of DON in TDN (%DON) was calculated by [DON]/[TDN] × 100 on a nitrogen basis.

**2.4. Optical index and parallel factor analysis**

We calculated optical indices, such as the spectral slope ($S_{275–295}$), DOC-specific ultraviolet absorbance ($SUVA_{254}$), and commonly used fluorescence-based indices (Gabor et al., 2014; Helms et

al., 2008; Weishaar et al., 2003), from the absorbance and EEM data to estimate the structural properties and origin of DOM (See Supporting Information, SI 1, Figs S3–S5). Other spectral slope indices that use longer wavelengths were not used because many samples were optically too dilute for the accurate calculation. In addition, we analyzed the EEMs by parallel factor analysis (PARAFAC) to mathematically deconvolute them into distinct fluorescent components with independent spectral characteristics (SI 2) (Murphy et al., 2018). The identified seven fluorescent components were compared with the published data on an open-access spectral database (OpenFluor; Murphy et al., 2014), with the Tucker congruence coefficient (TCC) as similarity criteria. The components were named according to their rounded fluorescence emission maximum: $C_{325}$, $C_{415}$, $C_{360}$, $C_{500}$, $C_{440}$, $C_{460}$, and $C_{300}$, with variation explained by each component decreasing sequentially from $C_{325}$ to $C_{300}$. $C_{300}$ was named so because it had a fluorescence maximum at Ex/Em = 270/302 nm when Em < 318 nm was not removed before modeling (data not shown). The fluorescence intensity at the maximum for each component was represented by Fmax (in RU) (Murphy et al., 2014). The Fmax of individual components divided by its DOC (Fmax/DOC) was calculated to track changes in its overall importance in the bulk DOM.

**2.5. Statistical Analysis**

The statistical difference between multiple parameters was tested by Tukey-Kramer's multiple

231 comparisons of means. Linear regressions were fitted using the ordinary least squares method with
232 log10 transformation of variables when needed. Correlations among Fmax/DOC values of the
233 identified PARAFAC components were evaluated using Spearman's rank correlation coefficient ($\rho$).
234 A significance level of 0.05 was selected for multiple comparisons to test the null hypothesis. Linear
235 correlations were considered statistically significant when $P < 0.01$. All analyses were conducted
236 with Origin 2016 (OriginLab Corporation, MA, USA).
237
238 **3. Results**
239 **3.1. Water chemistry and DOM composition**
240 Salinity of the samples ranged very broadly from fresh to hypersaline ($S$ = 179, 5 times that of
241 seawater; Table 1). The pH was neutral to slightly basic, and dissolved silica ($SiO_3^{2-}$) concentrations
242 were high (Table S2). Dissolved inorganic phosphorus and nitrogen concentrations were generally
243 very low and undetectable or below the quantification limit (Table S2). As a result, the %DON in
244 lakes was as high as 93.3% ± 13.6%. Among the measured nutrients, only $SiO_3^{2-}$ concentrations
245 increased along the salinity gradient of $S$ = 0–0.5, but the trend in $SiO_3^{2-}$ concentrations became
246 unclear in higher salinity lakes. Other nutrient concentrations did not show any trend along salinity.
247 The distribution patterns of C, N, and the absorption-based optical indices along the
248 salinity gradient are shown in Fig. 1. The DOC concentration ranged 0.25–146 mg C $L^{-1}$ and

249 increased as a function of salinity. A similar trend was observed for DON and $a_{254}$ (quantitative
250 measures of CDOM). Salinity alone explained 70%, 61%, and 53% of the variability of DOC, DON,
251 and $a_{254}$ values, respectively (linear regression of log-log plots). Consequently, a strong log-log
252 linear relationship was observed between DOC and $a_{254}$ ($R$ = 0.94, $P$ < 0.01) (Table 1). The low
253 DOC/DON ratios indicate the microbial origin of DOM. The %HPO ranged from 18.3% to 60.5%
254 (40.4% ± 8.5%). The %HPO tended to be lower in proglacial lakes and higher in the porewater of
255 lakes.

256 The UV-absorption indices ($SUVA_{254}$ and $S_{275–295}$) showed typical non-terrestrial
257 properties (Fig. 1, Table 2). The $SUVA_{254}$ values were low (0.22–1.66 L mg $C^{-1}$ $m^{-1}$) and did not
258 show a clear trend along salinity (Fig. 1e). Amundsen Lake 3, which receives large N inputs from the
259 catchment, had the highest $SUVA_{254}$ value among others (Fig. 1e). This lake had a very high
260 abundance of phytoplankton, which was obvious from its green color (Fig. S1f). We note that the
261 influence of $NO_3^-$ to the $SUVA_{254}$ value of this lake was negligible due to the low absorbance of
262 $NO_3^-$ ($A_{254}$ < 0.01 at 100 mg/L $NO_3^-$, Weishaar et al., 2003). In contrast, the values of $S_{275–295}$
263 showed a clear increasing tendency with the increase in salinity (log scale) ($R$ = 0.80, $P$ < 0.01; Fig.
264 1f). Porewater and stream samples had lower $S_{275–295}$ values than others at a given salinity (Fig. 1f,
265 Table 2). The fluorescent indices also showed typical non-terrestrial properties (Table 2), but values
266 varied along salinity in spite of the anticipated predominantly microbial origin of DOM (Fig. S6).

267

268 **3.2. Assignments of PARAFAC components**

269 Seven PARAFAC components were identified with our dataset (Fig. 2). For all of the components
270 except for $C_{300}$, multiple strong matches ($TCC_{ex \times em} > 0.95$) were observed (18, 23, 10, 40, 3, and 10
271 matches for $C_{325}$, $C_{415}$, $C_{360}$, $C_{500}$, $C_{440}$, and $C_{460}$, respectively) on OpenFluor. $C_{300}$ had seven
272 matching components with $TCC_{ex \times em} > 0.9$. Assignments of the components are summarized in Table
273 S3 with descriptions of each component provided in the past literature. Other than $C_{300}$, $C_{325}$, and
274 $C_{500}$, the identified components have been reported as either having allochthonous or autochthonous
275 origins (Table S3).

276 We assigned $C_{300}$ and $C_{325}$ as protein-like components (Table S3) based on their
277 fluorescence positions (Em < 350 nm) and the scarcity of polyphenols in Antarctic lakes. $C_{360}$ had
278 fluorescence peaks at Em 362 nm with the primary excitation maximum at 290 nm. The position of
279 $C_{360}$ was clearly different from a microbial humic-like component (peak M) that occurs at Em 370–
280 430 and Ex 290–325, which is often found in aquatic systems (Coble et al., 1998). Therefore, we
281 assigned this component as a non-humic peak N (Em 360–370 nm, Ex 280 nm), which has been
282 associated with new DOM production in water (Coble et al., 1998).

283 $C_{460}$ was assigned as a UVC humic-like component (Table S3), which was reported as
284 photorefractory because of the rapid attenuation of UVB light in water (Stedmon and Markager,

285 2005). The rest of the humic-like components ($C_{415}$, $C_{500}$, and $C_{440}$) have been reported as ubiquitous
286 components, which are found in almost all environments and derived from both allochthonous and
287 autochthonous sources (Table S3) (Murphy et al., 2018; Stedmon and Markager, 2005). We further
288 compared our model to the "ubiquity" models of Murphy et al. (2018), which were modeled by the
289 one-sample PARAFAC of a set of photo-decomposed DOM isolates (Fig. S7). Quite good matches
290 were found between $C_{415}$, $C_{500}$, and $C_{440}$ with several ubiquitous components in their models,
291 supporting our assertion that these components were ubiquitous humic-like components.
292
293 **3.3. Distribution of PARAFAC components**
294 Fluorescence intensity of the PARAFAC components (Fmax) less clearly increased along the salinity
295 gradient than the other quantitative measures (Fig. S8a), and salinity explained less than 42% of the
296 variability of Fmax (linear regression of log-log plots). The explained variability was especially
297 small for the ubiquitous humic-like components (5.7%–8.2%). When normalized by DOC, $C_{325}$ had
298 the highest intensities followed by $C_{415}$, while the other components had lower intensities and they
299 were not significantly different from each other (Fig. S9). It was evident that Fmax/DOC values of
300 the PARAFAC components differed among water types (Fig. S8b). Porewater samples typically had
301 a 5–20 times higher average Fmax/DOC values than lake surface water samples, except for $C_{460}$ and
302 $C_{300}$ (Table 2). Stream samples also had 2–9 times higher average Fmax/DOC values than lake

303 samples for the ubiquitous humic-like components ($C_{415}$, $C_{500}$, and $C_{440}$) (Table 2). Saline lake
304 samples had the lowest average Fmax/DOC values for all the components (Table 2).
305 Figure 3 was informative regarding the distribution of the PARAFAC components in
306 response to photodegradation, which was assessed by the spectral slope $S_{275–295}$ (Fichot and Benner,
307 2012; Helms et al., 2008): 1) $C_{360}$, which is derived from recent in-situ production (Coble et al.,
308 1998), did not show changes in its relative abundance depending on the degree of photodegradation
309 (Fig. 3b); 2) photodegradation decreased the ubiquitous humic-like components ($C_{415}$, $C_{500}$, and
310 $C_{440}$), and these components dominated more in the porewater and streams and less at the epilimnion
311 in saline lakes (Fig. 3c); 3) UVC humic-like component $C_{460}$, which is photorefractory (Stedmon and
312 Markager, 2005), increased its relative importance as photodegradation of bulk DOM progressed
313 (Fig. 3d); 4) Saline lakes exhibited unique PARAFAC compositions with more contribution from
314 protein-like components ($C_{325}$ and $C_{300}$) and much less contribution from $C_{460}$, which deviated from
315 the relationship between $\%C_{460}$ and $S_{275–295}$ (Figs. 3a and 3d); and 5) Amundsen Lake 3 (“penguin”
316 lake), which received substantial nutrient inputs from nearby penguin colonies (Table S2), had the
317 lowest protein-like components and highest ubiquitous humic-like components as well as
318 high $\%C_{360}$.
319
320 **4. Discussion**

### 4.1. Factors controlling DOM and nutrient concentrations

It was obvious that the bulk DOM concentration was significantly influenced by evapo-concentration in the Lützow-Holm Bay and Amundsen Bay lakes because of the dry climate (Figs. 1a and 1b). This was as expected because evapo-concentration or dilution by melt water inputs results in either the increase or decrease of any solute in water in closed hydrologic systems. Similar concentration effects have been observed in lower latitude arid regions. Among such studies, Osburn et al. (2011) compared DOC-conductivity (in mS $cm^{-1}$) relationships among saline lakes reported in past studies and found that the slope of regressions between log DOC and log conductivity varied from 0.322 to 0.796 (0.577 ± 0.156, n = 6). Our Antarctic lake samples had an equation of log DOC = 0.345 + 0.394 × log conductivity ($R^2$ = 0.68, $P$ < 0.001). The shallower slope of the regression compared to those reported in lower latitude arid regions suggested that the net DOM accumulation in the studied Antarctic lakes was lower, possibly due to the lack of nutrients necessary for primary production in lake water (Table S2) and the harsh Antarctic environment.

In contrast, nutrients other than dissolved silica were not concentrated by evapo-concentration (Table S2). Consequently, there were no correlations between the Fmax values of the PARAFAC components and nutrient concentrations, as opposed to those observed in arid lakes (Osburn et al., 2011). This implies that the Antarctic lakes are substantially N- and P-deficient compared to the arid lakes, rendering them oligotrophic (Kudoh and Tanabe, 2014). As a

result, %DON was more influenced by nutrient inputs from the surrounding areas than by evapo-concentration. For example, two lakes in Amundsen Bay (Amundsen Lake 1 and 3) had low %DON and had high nitrate ($NO_3^-$) concentrations because of N inputs from surrounding penguin colonies and south polar skua nests (Table S2). Similarly, five lakes (lakes other than Nurume) and the streams located in Yukidori and Yatsude Valleys in Langhovde are affected by inputs from abundant snow petrels that nest in the valleys and had low %DON (Table S2). These results suggested that the animal-related point source is important in influencing the nutrient distribution in Antarctic lakes.

**4.2. Factors controlling the DOM composition**

It appeared that both in-situ production and photodegradation substantially influenced the composition of DOM in the studied Antarctic lakes. The observed increase in $S_{275–295}$ values with increasing salinity (Fig. 1f) suggests the progression of photodegradation of DOM as a result of prolonged water retention time (Fichot and Benner, 2012; Helms et al., 2008). Most of $S_{275–295}$ values were higher than those previously reported in coastal waters where terrestrial inputs are low (for example, 0.024 $nm^{-1}$ in nearshore water of Georgia Bright; Helms et al., 2008), which supports the predominantly microbial (autochthonous) origin and/or the highly photodegraded state of the studied DOM. We note that the effects of salinity and pH on the optical properties were investigated

and found to be negligible (Table S4); thus, the compositional change was the primary driver for variability in CDOM and FDOM properties. The negligible effect of water chemistry on $S_{275–295}$ was particularity important because we used the index as the only indicator for DOM photodegradation. Fichot and Benner (2012) has also shown that neither biological processes nor changes in pH, ionic strength, $NO_3^-$, or $NO_2^-$ interferes with $S_{275–295}$ determination.

The distribution patterns of the PARAFAC components along $S_{275–295}$ (Fig. 3) could largely be interpreted by the following three biogeochemical processes: **i)** in-situ production, **ii)** photodegradation, and **iii)** precipitation due to high salinity. The four samples that had the top four highest $\%C_{360}$ (Fig. 3b) were those having the highest nutrient (especially $NO_3^-$, $NH_4^+$, and $PO_4^{3-}$) concentrations among others (Table S2), and water color of these lakes were yellow-green to green (Fig. S1f), strongly supporting that $C_{360}$ was derived from recent in-situ production. It is worth noting that there were stronger log-log correlations between DON concentrations with the levels of $C_{360}$ ($R = 0.73$) and the protein-like components ($R = 0.79–0.81$) than with those of the ubiquitous humic-like components ($R = 0.45–0.51$). Thus, we propose that the level of $C_{360}$ in the studied Antarctic lakes was primarily driven by in-situ production, and not by photodegradation. It is currently not established whether $C_{360}$ (Peak N) is directly produced by phytoplankton or requires bacterial processing of organic matter originated from primary production. However, the occurrence of Peak N in axenic diatom cultures does indicate that some phytoplankton can produce Peak N

directly (Castillo et al., 2010).

Photodegradation substantially influenced the relative contribution of the ubiquitous humic-like components and $C_{460}$ (Figs. 3c and 3d). This was in accordance with the photolabile and photorefractory nature of the ubiquitous humic-like components and $C_{460}$, respectively (Murphy et al., 2018; Stedmon and Markager, 2005). A decrease in %C(ubiquitous humic) (and their Fmax/DOC) at the epilimnion of saline lakes further supported the photodegradation of the ubiquitous humic-like components (Fig. 3c). In shallow freshwater Sôya Coast lakes (≤ 3 m), Tanabe et al. (2010) observed that 45%–60% of photosynthetically active radiation (PAR, 400–700 nm) and 20%–60% of ultraviolet radiation (300–400 nm) reached the lake beds, implying that photodegradation of the ubiquitous humic-like components could occur throughout the water column. It was as expected that porewater samples had higher contribution from the photolabile ubiquitous humic-like components because of the lack of sunlight penetration into the lake sediment (less than 1 cm) (Fig. 5 of Tanabe et al. 2010). Interestingly, stream samples had similar optical characteristics as porewater samples, namely, high $SUVA_{254}$ and %C(ubiquitous humic) and low $S_{275–295}$ and $\%C_{460}$ (Figs. 1 and 3, Table 2). We presume that this was because the water residence time of the streams (at most a few days) was much shorter than the most of lakes (except for lakes directly fed by a glacier) and, thus, stream DOM was not photodegraded substantially. The continuous DOM inputs from decomposed, partially humified mosses within the stream and in stream banks (Kanda et al.,

393 2004) could also be a source of the ubiquitous humic-like components. The low $\%C_{460}$ in saline
394 lakes (Fig. 3d) and concomitant increases in %C(protein) (Fig. 3a) could be caused by precipitation
395 of $C_{460}$ due to high salinity (Sholkovitz, 1976). Another possibility may be the greater primary
396 production of protein-like DOM in saline lakes (Osburn et al., 2011). However, it appeared that this
397 was not true, because Lake Funazoko, which had the much higher nutrient concentrations than other
398 saline lakes (Table S2), had lower C(protein)/DOC and thus lower %C(protein). Also, the phototroph
399 abundance is typically small in the studied saline lakes (Tanabe, unpublished data).
400 The lack of correlations between the protein-like component levels and nutrient
401 concentrations may be due to rapid microbial processing of the protein-like components originated
402 from primary production (Stedmon and Markager, 2005). It could also be partly due to the timing of
403 sampling. In Lakes Oyako and Hotoke in Sôya Coast, Tanabe et al. (2008) observed the maximum
404 chlorophyll a fluorescence under dim-light conditions during austral spring and autumn and the
405 minimum chlorophyll a fluorescence in ice-free summer, and they concluded that the too strong
406 summer light acts as an inhibitor of Antarctic phytoplankton growth. Since our samples were
407 collected during austral summer, they may have already undergone extensive algae breakdown and
408 photolytic/microbial modification of primary production-derived DOM. Insight as to intra-annual
409 variation of DOM concentrations and compositions should be gained when samples collected during
410 the winter time are analyzed. Finally, the fluorescence-based indices failed to adequately capture the

411 changes in FDOM compositions described above (Fig. S10).

412

413 **4.3. Generation of ubiquitous humic-like components and its ecological implications**

414 The evapo-concentration of the studied lakes occurs at variable rates reflecting the balance between
415 evaporation and freshwater inputs. As such, the correlation analysis of the fluorescence intensities of
416 the PARAFAC components would result in false-positive if not corrected for concentration effects.
417 Therefore, we compared the levels of the PARAFAC components after dividing by the DOC
418 concentrations (Fmax/DOC), as the DOC concentrations in this study were largely (70%) explained
419 by salinity and dividing by DOC could effectively reduce concentration effects. In addition,
420 Fmax/DOC represents the relative abundance of the PARAFAC components in the bulk DOM. Thus,
421 if Fmax/DOC values of two components vary and are strongly correlated among samples, it means
422 that the components behave in parallel independent of the behavior of the other constituents of DOM.
423 Figure 4 shows the correlations between $C_{360}$/DOC and the ubiquitous humic-like components
424 $C_{415}$/DOC, $C_{440}$/DOC, and $C_{500}$/DOC. All the ubiquitous humic-like components had a significant
425 strong correlation with $C_{360}$, while the other protein-like components and $C_{460}$ had a much weaker
426 correlation. The y-intercepts for $C_{415}$ and $C_{500}$ were not statistically different from zero ($P > 0.01$).
427 These universal correlations were observed despite the fact that the samples were collected from
428 closed hydrologic systems of distinct water types and different ice-free areas. This strongly

429 suggested that there were common processes that generated the ubiquitous components ($C_{415}$, $C_{440}$,
430 and $C_{500}$) from $C_{360}$ in the Lützow-Holm Bay and Amundsen Bay lakes and streams, with a certain
431 proportion of $C_{360}$ being transformed into the ubiquitous components. The inconsistent assignments
432 of these components in literature (allochthonous or autochthonous, Table S3) also imply their
433 multiple origins or common environmental processing that ultimately leads to these fluorescence.
434 Because the lakes have been isolated from each other (~7000 years) with independent water
435 catchment areas and they function as closed hydrologic systems, such a process should work on
436 areas larger than the catchment in size or it should work commonly among lakes.

437 In water, humic-like fluorophores can be generated in a culture of bacterial communities
438 amended with phytoplankton-derived DOM or simple substrates, such as glucose, in a relatively
439 short period (< a few weeks) (Kramer and Herndl, 2004; Rochelle-Newall and Fisher, 2002;
440 Shimotori et al., 2012). The bacterial processing of $C_{360}$ could be a source of the ubiquitous
441 humic-like fluorophores in the studied lakes. Although $C_{500}$ has not been linked to autochthonous
442 sources (Table S3), its relatively high contribution to our Antarctic dataset suggested that it was of
443 autochthonous origin in this study, re-emphasizing that one cannot assign humic-like fluorophores as
444 terrestrial just because their spectral features resemble that of terrestrially-derived natural organic
445 matter (Murphy et al., 2018). The fact that the same ubiquitous humic-like fluorophores were found
446 in Lake Fryxell and the deep Sargasso Sea (4534 m) (Fig. S7), where sunlight penetration is

447 negligible (discussed below), supports the biotic generation of these fluorophores. Although recent
448 studies demonstrated that humic-like fluorophores can also be generated directly from phytoplankton
449 in axenic cultures (Castillo et al., 2010; Chari et al., 2013; Fukuzaki et al., 2014), its contribution to
450 the generation of the ubiquitous humic-like fluorophores was likely low in our study considering the
451 lack of relationships between nutrient concentrations and ubiquitous humic-like fluorophore levels.
452 Furthermore, abiotic photochemical humification (photohumification) of DOM in the
453 presence of dissolved nitrogen has also been proposed (Kieber et al., 1997). Phootoxidation has been
454 shown to cross-link lipid precursors, incorporating N (free amine groups or ammonia) into the newly
455 formed marine humic substance and creating humic-like fluorescence (Kieber et al., 1997). Although
456 McKnight et al. (1991) noted that photohumification would not occur in McMurdo Dry Valleys
457 Antarctic lakes (such as Lake Fryxell), which are permanently ice-covered and thus have low light
458 intensities (photon flux density is 3–10 μmol photons $m^{-2}$ $s^{-1}$ below the ice) (McKnight et al., 1991),
459 it could occur in Lützow-Holm Bay and Amundsen Bay lakes because most lakes are completely
460 ice-free during the 2-month austral summer and they can have two orders brighter light (> 600 μmol
461 photons $m^{-2}$ $s^{-1}$ PAR up to 4 m) (Tanabe et al., 2008) than the lakes in McMurdo Dry Valleys.
462 Considering the richness of DON (Fig. 1) and the strong light intensity, photohumification in the
463 presence of DON (and DIN in some nutrient-rich lakes) may play an important role in abiotic
464 transformation of microbial DOM into distinct humic-like fluorophores in the studied Antarctic lakes.

The %HPO in this study (40.4% ± 8.5%) was generally higher than previously reported for lakes in the McMurdo Dry Valleys (Lake Vida, 12%–17%; Lakes Fryxell and Hoare; 17%–24% and 16%–18% as fulvic acid, respectively) and on Ross Island of East Antarctica (Pony Lake, 23%–34%) (Aiken et al., 1996; Cawley et al., 2016, 2013; McKnight et al., 1991), and similar to that of temperate clear water lakes (Table 1 of Sato et al., 2019). The higher %HPO of our samples than of lakes in the McMurdo Dry Valleys suggested the higher abundance of humic substances in the Lützow-Holm Bay and Amundsen Bay lakes and streams despite prevailing photodegradation. Levels of the ubiquitous humic-like components in the studied Antarctic lakes may reflect the balance between the abiotic/biotic production and photodegradation.

The ecological importance of CDOM in Antarctic lakes has been discussed mainly on its light-shading effect for primary producers (McKnight et al., 1994). The formation of humic-like fluorophores could be very important in regulating the depth of the euphotic zone to which visible wavelength radiation can penetrate. This light-shading role that CDOM plays in the studied lakes will be assessed in the future when we will finish analyzing the light penetrating properties of each lake. Another important attribute of Antarctic DOM could be its influence on the position of the thermocline. An example where DOM substantially influenced the thermocline depth could be seen from the depth trend in the water temperature of a saline lake Funazoko (Fig. S2k). The water temperature of Lake Funazoko showed a drastic change; it was approximately 6.8℃ at the surface,

483 increased to 20℃ at 1.7 m, then linearly decreased to −5℃ at 6.8 m. Because the depth trend in
484 conductivity did not correspond with that of temperature, the stratification was not a halocline but a
485 thermocline, in contrast to other saline lakes (Figs. S2 i, j, l). The very high DOC concentration (92.8
486 mg C $L^{-1}$) and absorption coefficient ($a_{254}$ = 96.1 $m^{-1}$) of the surface water of this lake (Table 1)
487 likely absorbed sunlight energy and increased the temperature. The depth trend in the temperature
488 was likely the balance between heating by the sunlight absorption and cooling by the atmosphere
489 and deeper water.
490
491 **5. Concluding remarks**
492 We found large compositional diversity in our Antarctic samples in terms of DOC/DON, %HPO,
493 UV-absorbing characteristics ($SUVA_{254}$ and $S_{275–295}$), and FDOM compositions, and such diversity
494 was largely due to a different degree of photodegradation. Therefore, the hypothesis that DOM in the
495 Antarctic lakes and streams has large compositional diversity and such diversity is mostly introduced
496 by external factors such as photodegradation was confirmed in our study. In addition, we proposed
497 that there were common processes that generated the ubiquitous humic-like components from $C_{360}$
498 (traditionally defined as Peak N) in the Lützow-Holm Bay and Amundsen Bay lakes and streams.
499 Although we consider biotic and photochemical processes primarily responsible for the generation of
500 the ubiquitous humic-like components, more studies are needed to elucidate the underlying

501 mechanisms.

502 We note that the CDOM and FDOM mainly studied in this work only captured a small
503 portion of the bulk DOM. Future work should broaden the analytical window and incorporate
504 chemical structural techniques, such as high-field nuclear magnetic resonance spectroscopy and
505 Fourier-transformed ion cyclotron resonance mass spectrometry, to unravel the unique chemistry of
506 Antarctic DOM, which should lead to a better understanding of the other pristine lakes in the world
507 and lower latitude aquatic systems as well.

508

509 **Acknowledgements**

510 We thank Kathleen Murphy and Urban Wünsch for discussion on PARAFAC modeling during the
511 19th International Conference of IHSS in Bulgaria. M.K. thanks IHSS for giving this opportunity
512 through the provision of Travel Support Awards. We are indebted to all those who provided essential
513 logistical support in the field during the 58th Japanese Antarctic Research Expedition. This study
514 was financially supported by JSPS KAKENHI 16H05885.

515

516 **References**

517 Aiken, G., McKnight, D., Harnish, R., Wershaw, R., 1996. Geochemistry of aquatic humic substances in
518 the Lake Fryxell Basin, Antarctica. Biogeochemistry 34, 157–188.

519 https://doi.org/10.1007/BF00000900

520 Castillo, C.R., Sarmento, H., Álvarez-Salgado, X.A., Gasol, J.M., Marraséa, C., 2010. Production of
521 chromophoric dissolved organic matter by marine phytoplankton. Limnol. Oceanogr. 55, 446–454.
522 https://doi.org/10.4319/lo.2010.55.1.0446

523 Cawley, K.M., McKnight, D.M., Miller, P., Cory, R., Fimmen, R.L., Guerard, J., Dieser, M., Jaros, C.,
524 Chin, Y.-P., Foreman, C., 2013. Characterization of fulvic acid fractions of dissolved organic matter
525 during ice-out in a hyper-eutrophic, coastal pond in Antarctica. Environ. Res. Lett. 8, 1–10.
526 https://doi.org/10.1088/1748-9326/8/4/045015

527 Cawley, K.M., Murray, A.E., Doran, P.T., Kenig, F., Stubbins, A., Chen, H., Hatcher, P.G., McKnight,
528 D.M., 2016. Characterization of dissolved organic material in the interstitial brine of Lake Vida,
529 Antarctica. Geochim. Cosmochim. Acta 183, 63–78. https://doi.org/10.1016/j.gca.2016.03.023

530 Chari, N.V.H.K., Keerthi, S., Sarma, N.S., Pandi, S.R., Chiranjeevulu, G., Kiran, R., Koduru, U., 2013.
531 Fluorescence and absorption characteristics of dissolved organic matter excreted by phytoplankton
532 species of western Bay of Bengal under axenic laboratory condition. J. Exp. Mar. Bio. Ecol. 445,
533 148–155. https://doi.org/10.1016/j.jembe.2013.03.015

534 Coble, P.G., Del Castillo, C.E., Avril, B., 1998. Distribution and optical properties of CDOM in the
535 Arabian Sea during the 1995 Southwest Monsoon. Deep Sea Res. Part II Top. Stud. Oceanogr. 45,
536 2195–2223. https://doi.org/10.1016/S0967-0645(98)00068-X

537 Farzadnia, S., Nimmagadda, R.D., McRae, C., 2017. A comparative structural study of nitrogen-rich
538 fulvic acids from various Antarctic lakes. Environ. Chem. 14, 502. https://doi.org/10.1071/EN17095
539 Fichot, C.G., Benner, R., 2012. The spectral slope coefficient of chromophoric dissolved organic matter
540 ( S 275-295 ) as a tracer of terrigenous dissolved organic carbon in river-influenced ocean margins.
541 Limnol. Oceanogr. 57, 1453–1466. https://doi.org/10.4319/lo.2012.57.5.1453
542 Findlay, S.E.G., Sinsabaugh, R.L., 2003. Aquatic Ecosystems, Academic Press. Elsevier.
543 https://doi.org/10.1016/B978-0-12-256371-3.X5000-8
544 Fukuzaki, K., Imai, I., Fukushima, K., Ishii, K.-I., Sawayama, S., Yoshioka, T., 2014. Fluorescent
545 characteristics of dissolved organic matter produced by bloom-forming coastal phytoplankton. J.
546 Plankton Res. 36, 685–694. https://doi.org/10.1093/plankt/fbu015
547 Gabor, R.S., Baker, A., McKnight, D.M., Miller, M.P., 2014. Fluorescence indices and their interpretation,
548 in: Aquatic Organic Matter Fluorescence. pp. 303–339.
549 https://doi.org/10.1017/CBO9781139045452.015
550 Hedges, J.I., Keil, R.G., Benner, R., 1997. What happens to terrestrial organic matter in the ocean? Org.
551 Geochem. 27, 195–212. https://doi.org/10.1016/S0146-6380(97)00066-1
552 Helms, J.R., Stubbins, A., Ritchie, J.D., Minor, E.C., Kieber, D.J., Mopper, K., 2008. Absorption spectral
553 slopes and slope ratios as indicators of molecular weight, source, and photobleaching of
554 chromophoric dissolved organic matter. Limnol. Oceanogr. 53, 955–969.

https://doi.org/10.4319/lo.2008.53.3.0955

Imura, S., Bando, T., Seto, K., Ohtani, S., 2003. Distribution of aquatic mosses in the Soya Coast region, East Antarctica. Polar Biosci. 16, 1–10.

Kanda, H., Imura, S., Ueno, T., 2004. On the structures of moss colony in the Yukidori Valley, Langhovde, East Antarctica. Polar Biosci. 17, 128–138.

Kida, M., Tanabe, M., Tomotsune, M., Yoshitake, S., Kinjo, K., Ohtsuka, T., Fujitake, N., 2019. Changes in dissolved organic matter composition and dynamics in a subtropical mangrove river driven by rainfall. Estuar. Coast. Shelf Sci. 223, 6–17. https://doi.org/10.1016/j.ecss.2019.04.029

Kieber, R.J., Hydro, L.H., Seaton, P.J., 1997. Photooxidation of triglycerides and fatty acids in seawater: Implication toward the formation of marine humic substances. Limnol. Oceanogr. 42, 1454–1462. https://doi.org/10.4319/lo.1997.42.6.1454

Kimura, S., Ban, S., Imura, S., Kudoh, S., Matsuzaki, M., 2010. Limnological characteristics of vertical structure in the lakes of Syowa Oasis, East Antarctica. Polar Sci. 3, 262–271. https://doi.org/10.1016/j.polar.2009.08.002

Kramer, G., Herndl, G., 2004. Photo- and bioreactivity of chromophoric dissolved organic matter produced by marine bacterioplankton. Aquat. Microb. Ecol. 36, 239–246. https://doi.org/10.3354/ame036239

Kudoh, S., Tanabe, Y., 2014. Limnology and ecology of lakes along the Sôya Coast, East Antarctica. Adv.

573 Polar Sci. 25, 75–91. https://doi.org/10.13679/j.advps.2014.1.00075

574 Matsumoto, G.I., 1989. Biogeochemical study of organic substances in Antarctic lakes. Hydrobiologia

575 172, 265–299. https://doi.org/10.1007/BF00031627

576 McKnight, D.M., Aiken, G.R., Smith, R.L., 1991. Aquatic fulvic acids in microbially based ecosystems:

577 results from two desert lakes in Antartica. Limnol. Oceanogr. 36, 998–1006.

578 McKnight, D.M., Andrews, E.D., Spaulding, S.A., Aiken, G.R., 1994. Aquatic fulvic acids in algal-rich

579 antarctic ponds. Limnol. Oceanogr. 39, 1972–1979. https://doi.org/10.4319/lo.1994.39.8.1972

580 Murphy, K.R., Stedmon, C.A., Wenig, P., Bro, R., 2014. OpenFluor- an online spectral library of

581 auto-fluorescence by organic compounds in the environment. Anal. Methods 6, 658–661.

582 https://doi.org/10.1039/c3ay41935e

583 Murphy, K.R., Timko, S.A., Gonsior, M., Powers, L.C., Wünsch, U.J., Stedmon, C.A., 2018.

584 Photochemistry illuminates ubiquitous organic matter fluorescence spectra. Environ. Sci. Technol.

585 52, 11243–11250. https://doi.org/10.1021/acs.est.8b02648

586 Osburn, C.L., Wigdahl, C.R., Fritz, S.C., Saros, J.E., 2011. Dissolved organic matter composition and

587 photoreactivity in prairie lakes of the U.S. Great Plains. Limnol. Oceanogr. 56, 2371–2390.

588 https://doi.org/10.4319/lo.2011.56.6.2371

589 Rochelle-Newall, E., Fisher, T.., 2002. Production of chromophoric dissolved organic matter fluorescence

590 in marine and estuarine environments: an investigation into the role of phytoplankton. Mar. Chem.

77, 7–21. https://doi.org/10.1016/S0304-4203(01)00072-X

Roth, V., Dittmar, T., Gaupp, R., Gleixner, G., 2014. Ecosystem-specific composition of dissolved organic matter. Vadose Zo. J. 13, 10p. https://doi.org/10.2136/vzj2013.09.0162

Sato, H., Kida, M., Yamano, S., Sonoda, H., Fujitake, N., 2019. Variable relationships between the hydrophobic fraction of dissolved organic matter and metals in Scottish freshwater before the estuarine mixing zone. Limnology. https://doi.org/10.1007/s10201-018-0569-8

Shimotori, K., Watanabe, K., Hama, T., 2012. Fluorescence characteristics of humic-like fluorescent dissolved organic matter produced by various taxa of marine bacteria. Aquat. Microb. Ecol. 65, 249–260. https://doi.org/10.3354/ame01552

Sholkovitz, E.R., 1976. Flocculation of dissolved organic and inorganic matter during the mixing of river water and seawater. Geochim. Cosmochim. Acta 40, 831–845. https://doi.org/10.1016/0016-7037(76)90035-1

Stedmon, C., Markager, S., 2005. Resolving the variability in dissolved organic matter fluorescence in a temperate estuary and its catchment using PARAFAC analysis. Limnol. Oceanogr. 50, 686–697. https://doi.org/10.4319/lo.2005.50.2.0686

Takahashi, A., Sato, K., Nishikawa, J., Kouno, M., Naito, Y., 2000. Distribution and size of Adelie penguin colonies in Amundsen Bay, Enderby Land, Antarctica. Antarct. Rec. 44, 38–41. https://doi.org/doi/10.15094/00009113

609 Tanabe, Y., Kudoh, S., Imura, S., Fukuchi, M., 2008. Phytoplankton blooms under dim and cold
610 conditions in freshwater lakes of East Antarctica. Polar Biol. 31, 199–208.
611 https://doi.org/10.1007/s00300-007-0347-2
612 Tanabe, Y., Ohtani, S., Kasamatsu, N., Fukuchi, M., Kudoh, S., 2010. Photophysiological responses of
613 phytobenthic communities to the strong light and UV in Antarctic shallow lakes. Polar Biol. 33, 85–
614 100. https://doi.org/10.1007/s00300-009-0687-1
615 Tanabe, Y., Yasui, S., Osono, T., Uchida, M., Kudoh, S., Yamamuro, M., 2017. Abundant deposits of
616 nutrients inside lakebeds of Antarctic oligotrophic lakes. Polar Biol. 40, 603–613.
617 https://doi.org/10.1007/s00300-016-1983-1
618 Weishaar, J.L., Aiken, G.R., Bergamaschi, B.A., Fram, M.S., Fujii, R., Mopper, K., 2003. Evaluation of
619 specific ultraviolet absorbance as an indicator of the chemical composition and reactivity of
620 dissolved organic carbon. Environ. Sci. Technol. 37, 4702–4708. https://doi.org/10.1021/es030360x
621 Zark, M., Christoffers, J., Dittmar, T., 2017. Molecular properties of deep-sea dissolved organic matter are
622 predictable by the central limit theorem: Evidence from tandem FT-ICR-MS. Mar. Chem. 191, 9–
623 15. https://doi.org/10.1016/j.marchem.2017.02.005
624 Zark, M., Dittmar, T., 2018. Universal molecular structures in natural dissolved organic matter. Nat.
625 Commun. 9, 8p. https://doi.org/10.1038/s41467-018-05665-9
626

**Table 1.** The sampling locations, limnological characteristics, and basic optical and chemical properties of DOM for each lake of Lützow-Holm Bay and Amundsen Bay ice-free area.

| Area name | Lake name | Type | Water type | Altitude (m) | Length (km) | Area ($\times 10^4$ m$^2$) | Catchment area ($\times 10^4$ m$^2$) | Maximum depth (m) | Sampling depth (m) | Sampling date | Salinity | pH | Temp. (°C) | DOC (mg C L$^{-1}$) | %HPO (%) | $a_{254}$ (m$^{-1}$) |
|---|---|---|---|---|---|---|---|---|---|---|---|---|---|---|---|---|
| A | Amundsen Lake1 | ND | others | ND | 0.34 | 1.3 | ND | 0.5 | shore | 19 Feb. 2017 | 0.035 | 6.97 | 3.9 | 0.76 | 59.2 | scatter |
| A | Amundsen Lake2 | ND | others | ND | 0.13 | 0.6 | ND | ND | shore | 23 Feb. 2017 | 0.030 | 7.87 | 2.7 | 2.00 | 45.2 | 4.42 |
| A | Amundsen Lake3 | ND | others | ND | 0.15 | 0.2 | ND | ND | shore | 23 Feb. 2017 | 0.193 | 10.5 | 3.5 | 11.1 | 43.6 | 42.4 |
| A | Richardson | ND | proglacial | ND | 4.76 | 544 | ND | ND | shore | 19 Feb. 2017 | 0.023 | 6.59 | 3.5 | 1.16 | 30.1 | scatter |
| B | Hiroe | 3 | proglacial | ***215*** | 0.96 | 35.2 | ND | ***9.5*** | 4.0 | 19 Jan. 2017 | 0.016 | 7.84 | 2.9 | 0.36 | 46.5 | 0.60 |
| B | Breivagnipa Lake1 | 3 | proglacial | 285 | 0.15 | 0.6 | ND | ND | shore | 19 Jan. 2017 | 0.198 | 7.86 | 6.4 | 1.36 | 36.0 | 2.04 |
| L | Yukidori | ***3*** | others | ***125*** | ***0.28*** | ***4.1*** | ND | ***8.6*** | 3.5 | 10 Jan. 2017 | 0.034 | 8.22 | 6.6 | 0.89 | 48.0 | 0.71 |
| L | Yukidori | ***3*** | pore | 125 | ***0.28*** | ***4.1*** | ND | ***8.6*** | pore | 10 Jan. 2017 | 0.311 | ND | ND | 3.73 | 57.3 | 10.2 |
| L | Mitsuike Ue | ND | others | 40 | 0.05 | 0.2 | 20.6 | 1.0 | shore | 13 Jan. 2017 | 0.606 | 8.36 | 7.8 | 1.67 | 32.1 | 2.63 |
| L | Mitsuike Naka | ND | others | 40 | 0.07 | 0.2 | 9.7 | 1.0 | shore | 13 Jan. 2017 | 0.794 | 8.24 | 8.2 | 1.22 | 29.2 | 1.68 |
| L | Mitsuike Shita | ND | others | 30 | 0.06 | 0.2 | 24.9 | 1.5 | shore | 13 Jan. 2017 | 0.879 | 8.39 | 8.2 | 2.22 | 31.0 | 3.55 |
| L | Nurume | ***1*** | saline | ***0*** | ***0.31*** | ***3.5*** | 17.4 | ***16.2*** | 3.0 | 12 Jan. 2017 | 29.1 | 8.13 | 6.6 | 2.24 | 40.7 | 3.56 |
| L | Nurume | ***1*** | saline | ***0*** | ***0.31*** | ***3.5*** | 17.4 | ***16.2*** | 8.5 | 12 Jan. 2017 | 32.2 | 8.13 | 3.2 | 6.21 | 40.7 | 10.4 |
| L | Nurume | ***1*** | saline | ***0*** | ***0.31*** | ***3.5*** | 17.4 | ***16.2*** | 14 | 12 Jan. 2017 | 54.7 | 7.17 | 2.1 | 11.2 | 48.4 | scatter |
| L | Heito | ***3*** | proglacial | ***165*** | 0.51 | 4.9 | ND | ***4.5*** | shore | 9 Jan. 2017 | 0.024 | 7.32 | 1.8 | 0.64 | 31.0 | 1.19 |
| R | Maruwan-Oike | ***2*** | proglacial | ***10*** | 0.63 | ***25.2*** | ND | ***37*** | 9.0 | 17 Jan. 2017 | 0.015 | 7.96 | 3.6 | 0.56 | 20.4 | scatter |
| R | Maruwan Kita | 2 | proglacial | 15 | ***0.20*** | ***4.6*** | ND | ND | shore | 17 Jan. 2017 | 0.016 | 7.44 | 2.3 | 1.02 | 18.3 | 1.04 |
| R | Maruwan Minami | ***2*** | proglacial | 15 | ***0.55*** | ***2.0*** | ND | ***11.5*** | shore | 17 Jan. 2017 | 0.022 | 7.15 | 5.2 | 0.72 | 27.6 | 0.47 |
| Sl | Skallen-Oike | ***2*** | others | 5 | 1.10 | 22.5 | 115.0 | ***9.2*** | 3.5 | 4 Jan. 2017 | 0.132 | 8.06 | 4.1 | 1.43 | 48.4 | 2.57 |
| Sl | Skallen-Oike | ***2*** | pore | 5 | 1.10 | 22.5 | 115.0 | ***9.2*** | pore | 4 Jan. 2017 | 0.138 | ND | ND | 7.86 | 58.7 | 19.7 |
| Sl | Skallen Lake1 | ND | others | 30 | 0.23 | 1.3 | ND | ND | shore | 4 Jan. 2017 | 0.072 | 8.14 | 6.5 | 0.71 | 40.5 | 1.34 |
| Sl | Skallen Lake2 | ND | others | 30 | 0.11 | 0.3 | ND | ND | shore | 4 Jan. 2017 | 0.050 | 8.40 | 8.6 | 0.78 | 30.1 | 1.92 |
| Sl | Skallen Lake3 | ND | others | 55 | 0.14 | 0.9 | ND | ND | shore | 5 Jan. 2017 | 0.078 | 8.50 | 6.0 | 1.25 | 35.9 | 1.87 |
| Sl | Skallen Lake4 | ND | others | 75 | 0.17 | 1.2 | ND | ND | shore | 5 Jan. 2017 | 0.040 | 8.48 | 9.5 | 0.71 | 32.0 | 0.67 |
| Sl | Skallen Lake5 | ND | others | 45 | 0.11 | 0.6 | ND | ND | shore | 5 Jan. 2017 | 0.034 | 8.22 | 10.1 | 1.07 | 37.6 | 2.57 |
| Sl | Glacial Lake | ND | proglacial | 10 | 0.34 | 4.6 | ND | ND | shore | 4 Jan. 2017 | 0.074 | 7.35 | 7.7 | 0.25 | 41.1 | scatter |
| Sl | Glacial Water | - | proglacial | 15 | - | - | - | - | melt | 4 Jan. 2017 | 0.017 | 6.52 | 1.5 | 0.33 | 30.4 | scatter |
| Sr | Oyako | ***2*** | others | ***5*** | ***0.43*** | ***6.5*** | 280.0 | ***8.0*** | 4.0 | 27 Dec. 2016 | 0.364 | 8.27 | 5.7 | 1.19 | 54.2 | 2.37 |
| Sr | Naga | ***3*** | others | ***70*** | ***0.38*** | ***4.8*** | 23.9 | ***10.8*** | 5.0 | 28 Dec. 2016 | 0.879 | 8.56 | 4.9 | 3.51 | 36.1 | 2.33 |
| Sr | Naga | ***3*** | pore | ***70*** | ***0.38*** | ***4.8*** | 23.9 | ***10.8*** | pore | 28 Dec. 2016 | 0.880 | ND | ND | ND | ND | 27.1 |
| Sr | Nyorai | ***3*** | others | ***130*** | 0.18 | 0.6 | 7.5 | ***3.0*** | 1.5 | 29 Dec. 2016 | 0.330 | 8.30 | 7.1 | 1.54 | 44.6 | 1.94 |
| Sr | Nyorai | ***3*** | pore | ***130*** | 0.18 | 0.6 | 7.5 | ***3.0*** | pore | 29 Dec. 2016 | 0.331 | ND | ND | 8.47 | ND | 18.3 |
| Sr | Hotoke | ***3*** | others | ***120*** | 0.12 | 0.4 | 6.7 | ***3.0*** | 1.0 | 30 Dec. 2016 | 0.421 | 8.31 | 4.8 | 1.08 | 40.5 | 1.66 |
| Sr | Hotoke | ***3*** | pore | ***120*** | 0.12 | 0.4 | 6.7 | ***3.0*** | pore | 30 Dec. 2016 | 1.018 | ND | ND | ND | ND | 19.5 |
| Sr | Kuwai | ***3*** | others | ***160*** | 0.08 | 0.3 | 4.0 | ***4.3*** | 2.0 | 30 Dec. 2016 | 1.608 | 7.57 | 10.3 | 0.94 | 38.3 | 1.19 |
| Sr | Bosatsu | ***3*** | others | ***130*** | 0.19 | 0.8 | 10.4 | ***4.8*** | 2.0 | 25 Jan. 2017 | 0.181 | 8.05 | 8.4 | 1.38 | 38.4 | 1.50 |

| | | | | | | | | | | | | | | | | |
|---|---|---|---|---|---|---|---|---|---|---|---|---|---|---|---|---|
| Sr | Jizo | ***3*** | others | ***120*** | 0.10 | 0.3 | 2.1 | ***3.1*** | 1.5 | 25 Jan. 2017 | 1.227 | 8.54 | 8.2 | 1.46 | 41.4 | 2.47 |
| Sr | Himago | 1 | others | −5 | 0.08 | 0.4 | 9.6 | ND | shore | 27 Jan. 2017 | 3.897 | 8.42 | 7.8 | 5.23 | 43.2 | 10.3 |
| Sr | Mago | ***1*** | others | ***−5*** | 0.18 | 1.1 | 35.3 | ***1.7*** | shore | 27 Jan. 2017 | 2.226 | 8.56 | 7.3 | 4.57 | 46.3 | 8.03 |
| Sr | Sara | ***1*** | others | ***0*** | 0.18 | 1.1 | 24.3 | ***2.5*** | 1.5 | 27 Jan. 2017 | 0.365 | 8.75 | 7.1 | 2.09 | 45.0 | 4.59 |
| Sr | Tokkuri | ***3*** | others | 45 | 0.24 | 1.9 | 65.5 | 6.0 | shore | 28 Jan. 2017 | 0.873 | 8.04 | 6.5 | 2.77 | 48.6 | 3.17 |
| Sr | Kumogata | ***3*** | others | 65 | 0.32 | *3.2* | 78.5 | 0.8 | shore | 28 Jan. 2017 | 0.648 | 7.42 | 6.3 | 3.90 | 37.6 | 4.25 |
| Sr | Hyotan | ***3*** | others | ***75*** | ***0.37*** | ***5.3*** | 40.0 | ***12.4*** | 6.0 | 31 Jan. 2017 | 1.070 | 8.80 | 5.9 | 2.69 | 42.6 | 2.44 |
| Sr | Hamagiku | ND | others | 95 | 0.28 | 1.9 | 10.5 | ***4.0*** | 2.0 | 31 Jan. 2017 | 0.064 | 8.05 | 4.2 | 0.90 | 38.5 | 1.33 |
| Sr | Ebi | ND | others | 50 | 0.31 | 2.2 | 31.8 | ***6.3*** | 3.0 | 31 Jan. 2017 | 0.842 | 8.81 | 5.3 | 2.94 | 40.3 | 2.89 |
| Sr | Kikuno | ND | others | 55 | 0.29 | 1.3 | 14.3 | 2.5 | shore | 31 Jan. 2017 | 1.232 | 8.53 | 4.9 | 1.75 | 36.9 | 2.44 |
| Sr | Hashioki | 1 | others | 10 | 0.26 | 1.2 | 34.1 | 2.0 | shore | 27 Jan. 2017 | 0.267 | 8.42 | 7.3 | 1.73 | 39.8 | 3.18 |
| Sr | Skarvsnes Lake2 | ND | others | 55 | 0.09 | 0.4 | 0.6 | ND | shore | 31 Jan. 2017 | 0.964 | 8.56 | 5.8 | 2.57 | 41.6 | 3.15 |
| Sr | A-5 | ND | others | 90 | 0.07 | 0.2 | 7.8 | 2.0 | shore | 31 Jan. 2017 | 0.392 | 8.59 | 5.1 | 3.36 | 38.6 | 5.38 |
| Sr | Hechima | ***3*** | others | ***85*** | 0.22 | 1.4 | 16.0 | ***6.3*** | shore | 6 Feb. 2017 | 1.669 | 8.73 | 5.2 | 1.43 | 44.8 | ND |
| Sr | Magobachi | ***3*** | others | ***60*** | 0.27 | 1.5 | 17.0 | ***5.0*** | shore | 6 Feb. 2017 | 1.017 | 8.83 | 5 | 1.27 | 44.9 | 2.12 |
| Sr | Misumi | ND | others | ***90*** | 0.13 | 0.7 | 6.1 | 6.3 | shore | 6 Feb. 2017 | 0.093 | 8.17 | 5 | 1.79 | 54.3 | 1.44 |
| Sr | Kobachi | ***1*** | saline | ***25*** | 0.34 | 4.4 | 75 | ***12*** | 1.5 | 27 Jan. 2017 | 7.37 | 8.86 | 7.2 | 4.39 | 42.9 | 5.62 |
| Sr | Kobachi | ***1*** | saline | ***25*** | 0.34 | 4.4 | 75 | ***12*** | 6.0 | 27 Jan. 2017 | 13.6 | 8.75 | 9.7 | 6.62 | 43.9 | 8.53 |
| Sr | Suribachi | ***1*** | saline | ***−33*** | 1.2 | 58.8 | 387 | ***32*** | 2.0 | 27 Jan. 2017 | 69.8 | 7.66 | 11.8 | 12.2 | 39.6 | 6.11 |
| Sr | Suribachi | ***1*** | saline | ***−33*** | 1.2 | 58.8 | 387 | ***32*** | 6.0 | 27 Jan. 2017 | 121 | 7.88 | 20.7 | 35.1 | 39.7 | 17.7 |
| Sr | Funazoko | ***1*** | saline | ***−23*** | 0.66 | 13.1 | 118 | ***9.2*** | 2.0 | 28 Jan. 2017 | 155 | 7.40 | 20.3 | 92.8 | 29.9 | 96.1 |
| Sr | Funazoko | ***1*** | saline | ***−23*** | 0.66 | 13.1 | 118 | ***9.2*** | 6.0 | 28 Jan. 2017 | 179 | 7.34 | −3.5 | 146 | 29.0 | 158 |

GPS data (Interactive Map file .kmz) are provided online.

ND = not determined, scatter = samples that contained clay-sized particles after filtration (0.3 μm) and thus absorbance data not presented, while that of Nurume 14 m was due to flocculation upon oxidation.

Length = longitudinal length, melt = glacier melt that drains into Glacial Lake, pore = porewater

Area name; A = Amundsen Bay, B = Breivågnipa, L = Langhovde, R = Rundvågshetta, Sl = Skallen, Sr = Skarvsnes.

Type = geographical type; 1 = Marine relict and lentic lakes, 2 = marine relict and lotic lakes, 3 = non-marine relict lakes.

Geographical and morphologic data in bold italics were compiled from (Kimura et al., 2010), (Kudoh and Tanabe, 2014), and (Imura et al., 2003).

Table 2. Average (standard error) values of the optical parameters in each water type.

| | $a_{254}$ | $SUVA_{254}$ | $S_{275–295}$ | FI | HIX | BIX | $C_{325}$/DOC | $C_{415}$/DOC | $C_{360}$/DOC | $C_{500}$/DOC | $C_{440}$/DOC | $C_{460}$/DOC | $C_{300}$/DOC |
|---|---|---|---|---|---|---|---|---|---|---|---|---|---|
| Water type | ($m^{-1}$) | (L mg $C^{-1}$ $m^{-1}$) | ($\times10^{-3}$ $nm^{-1}$) | | | | ($\times10^{-3}$ RU L mg $C^{-1}$) | ($\times10^{-3}$ RU L mg $C^{-1}$) | ($\times10^{-3}$ RU L mg $C^{-1}$) | ($\times10^{-3}$ RU L mg $C^{-1}$) | ($\times10^{-3}$ RU L mg $C^{-1}$) | ($\times10^{-3}$ RU L mg $C^{-1}$) | ($\times10^{-3}$ RU L mg $C^{-1}$) |
| Proglacial lake | $1.07^{a}$ | $0.579^{a}$ | $25.6^{ab}$ | $1.452^{a}$ | $0.335^{a}$ | $0.935^{a}$ | $38.9^{c}$ | $8.75^{c}$ | $7.69^{c}$ | $5.18^{c}$ | $2.12^{c}$ | $3.86^{bc}$ | $15.5^{a}$ |
| N = 5–9 | (0.62) | (0.211) | (5.35) | (0.098) | (0.070) | (0.100) | (21.7) | (4.43) | (3.80) | (3.62) | (1.04) | (1.79) | (8.80) |
| Saline lake | $38.2^{bc}$ | $0.486^{a}$ | $49.5^{c}$ | $1.776^{c}$ | $0.384^{ab}$ | $1.218^{b}$ | $9.29^{c}$ | $4.18^{c}$ | $4.00^{c}$ | $1.45^{c}$ | $0.98^{c}$ | $2.35^{c}$ | $6.43^{b}$ |
| N = 8–9 | (57.4) | (0.190) | (12.9) | (0.171) | (0.117) | (0.181) | (5.76) | (3.76) | (3.06) | (1.33) | (0.88) | (1.67) | (3.74) |
| Other lake[1] | $2.88^{a}$ | $0.652^{a}$ | $32.2^{b}$ | $1.581^{b}$ | $0.488^{c}$ | $0.900^{a}$ | $22.7^{c}$ | $9.87^{c}$ | $6.85^{c}$ | $4.49^{c}$ | $2.65^{c}$ | $7.39^{ab}$ | $9.80^{ab}$ |
| N = 32–33 | (2.00) | (0.206) | (6.76) | (0.086) | (0.074) | (0.054) | (12.9) | (4.81) | (3.82) | (2.44) | (1.48) | (3.02) | (5.21) |
| Porewater | $19.0^{ab}$ | $1.071^{c}$ | $18.1^{a}$ | $1.781^{c}$ | $0.481^{bc}$ | $0.936^{a}$ | $111^{a¥}$ | $91.4^{a}$ | $37.7^{a}$ | $23.9^{a}$ | $27.0^{a}$ | $6.56^{abc}$ | $13.4^{ab}$ |
| N = 3–5 | (6.02) | (0.124) | (0.48) | (0.062) | (0.105) | (0.060) | (4.05) | (23.5) | (12.0) | (1.90) | (4.43) | (1.83) | (1.29) |
| Stream | $1.09^{a}$ | $0.862^{bc}$ | $17.2^{a}$ | $1.569^{ab}$ | $0.573^{d}$ | $0.836^{a}$ | $37.9^{b}$ | $32.1^{b}$ | $11.3^{b}$ | $13.3^{b}$ | $8.58^{b}$ | $7.79^{a}$ | $12.1^{ab}$ |
| N = 16 | (0.33) | (0.200) | (3.05) | (0.088) | (0.099) | (0.060) | (11.6) | (14.9) | (3.76) | (6.01) | (4.61) | (3.11) | (6.37) |

[1] Excluding Amundsen Lake 3.

Different letters in each parameter indicate significant differences among water types at $P < 0.05$ based on Tukey-Kramer's multiple comparisons of means.

$a_{254}$ = absorption coefficient of dissolved organic matter at 254 nm, $SUVA_{254}$ = specific UV absorbance at 254 nm, $S_{275–295}$ = spectral slope determined between 275 nm and 295 nm, FI = fluorescence index, HIX = humification index, BIX = biological index, and $C_x$/DOC = fluorescence intensity of each PARAFAC component normalized by its sample dissolved organic carbon concentration

Fig. 1. Distribution of dissolved C or N properties (a–d) and UV absorption properties (e, f) of Lützow-Holm Bay and Amundsen Bay lake and stream samples along the salinity gradient (log scaled). Samples were categorized into six water types and represented by color. Open black circle ("penguin") represents a sample collected at Amundsen Lake 3 with abundant phytoplankton because of penguin guano inputs. Error bar for %HPO indicates one standard deviation of quadruplicate experiments. Correlation coefficients between log DOC, log DON, DOC/DON, $SUVA_{254}$, and $S_{275–295}$ with log salinity were 0.83, 0.78, 0.51, −0.38, and 0.80, respectively (all $P < 0.01$).

Fig. 2. Counter plots of three-dimensional spectra of the identified PARAFAC components from Lützow-Holm Bay and Amundsen Bay lake and stream samples. The components were named according to their rounded fluorescence emission maximum.

Fig. 3. Relationships between relative contribution of PARAFAC components and the spectral slope ($S_{275–295}$). %C(protein) = relative contribution of the sum of the protein-like components ($C_{325}$ and $C_{300}$), while %C(ubiquitous humic) = relative contribution of the sum of the ubiquitous humic-like components ($C_{415}$, $C_{500}$, and $C_{440}$). $C_{360}$ = analogous to traditional Peak N (Coble et al., 1998), while $C_{460}$ = photorefractory UVC humic-like component. Samples were categorized into six water types as in Fig. 1. Tentative interpretations on the pattern and directions of changes due to environmental processing (salinity-induced precipitation and photodegradation) are shown (see main text). In (b) and (c), saline lake samples are labeled as follows: S2 & 6 = Suribachi 2 & 6 m, F2 & 6 = Funazoko 2 & 6 m, K1.5 & 6 = Kobachi 1.5 & 6 m, N3 & 8.5 = Nurume 3 & 8.5 m, where numbers after the lake names represent the depths at which samples were collected (See Table 1).

Fig. 4. Correlation between $C_{360}$/DOC versus $C_{415}$/DOC, $C_{440}$/DOC, and $C_{500}$/DOC (ubiquitous humic-like fluorophore). The inset shows correlation matrix among the levels of the identified PARAFAC components (Fmax/DOC) with Spearman's correlation coefficient (ρ) indicated by color.

Figure 1

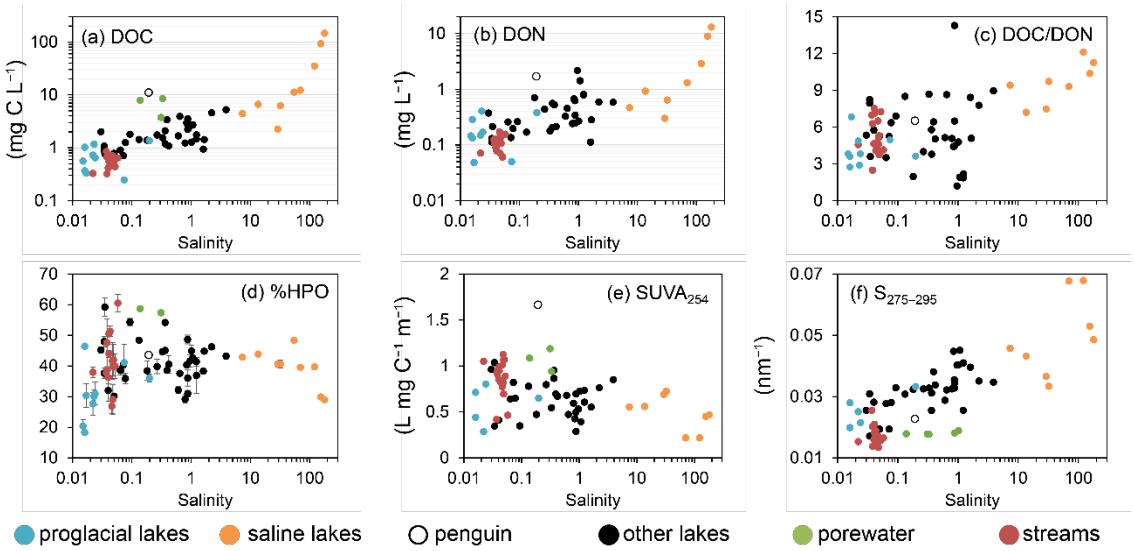


Figure 2

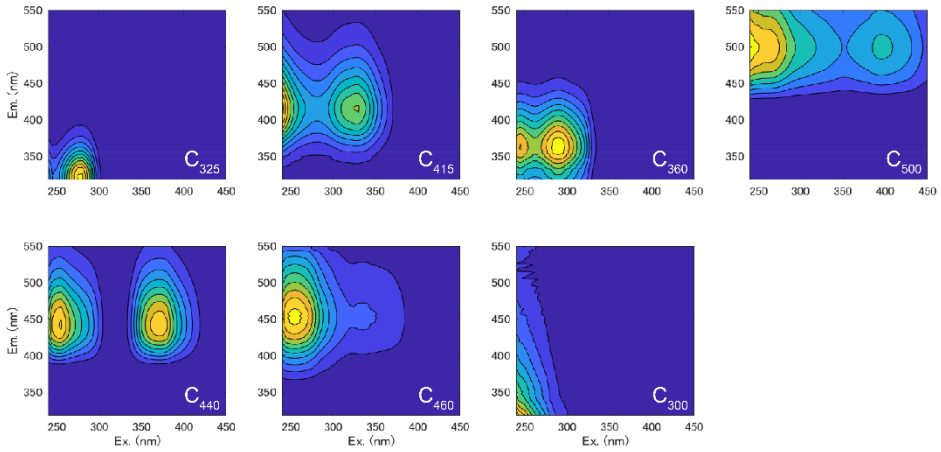

Figure 3

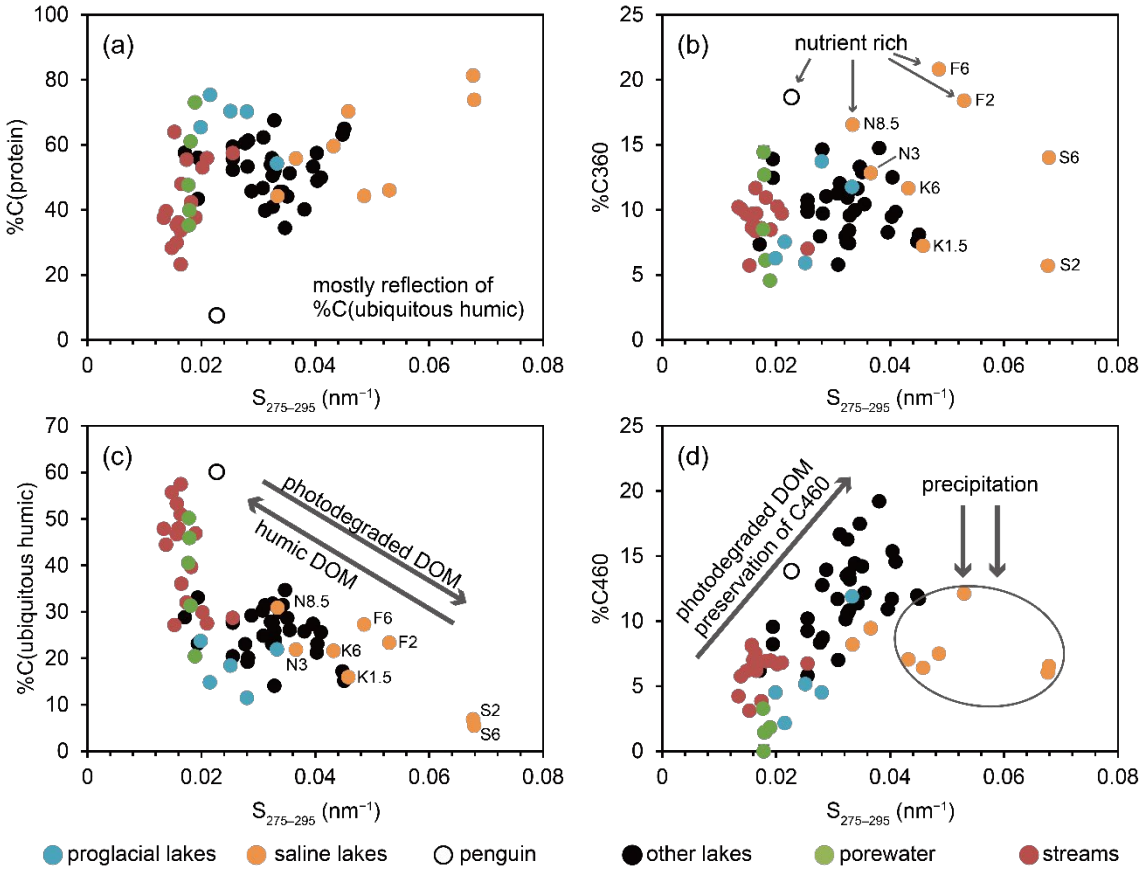
(a)
%C(protein)
mostly reflection of
%C(ubiquitous humic)
(b)
%C360
nutrient rich
F6
F2
N8.5
N3
S6
K6
K1.5
S2
(c)
%C(ubiquitous humic)
photodegraded DOM
humic DOM
N8.5
F6
F2
K6
N3
K1.5
S2
S6
(d)
%C460
photodegraded DOM
preservation of C460
precipitation
S275–295 (nm−1)
proglacial lakes
saline lakes
penguin
other lakes
porewater
streams

Figure 4

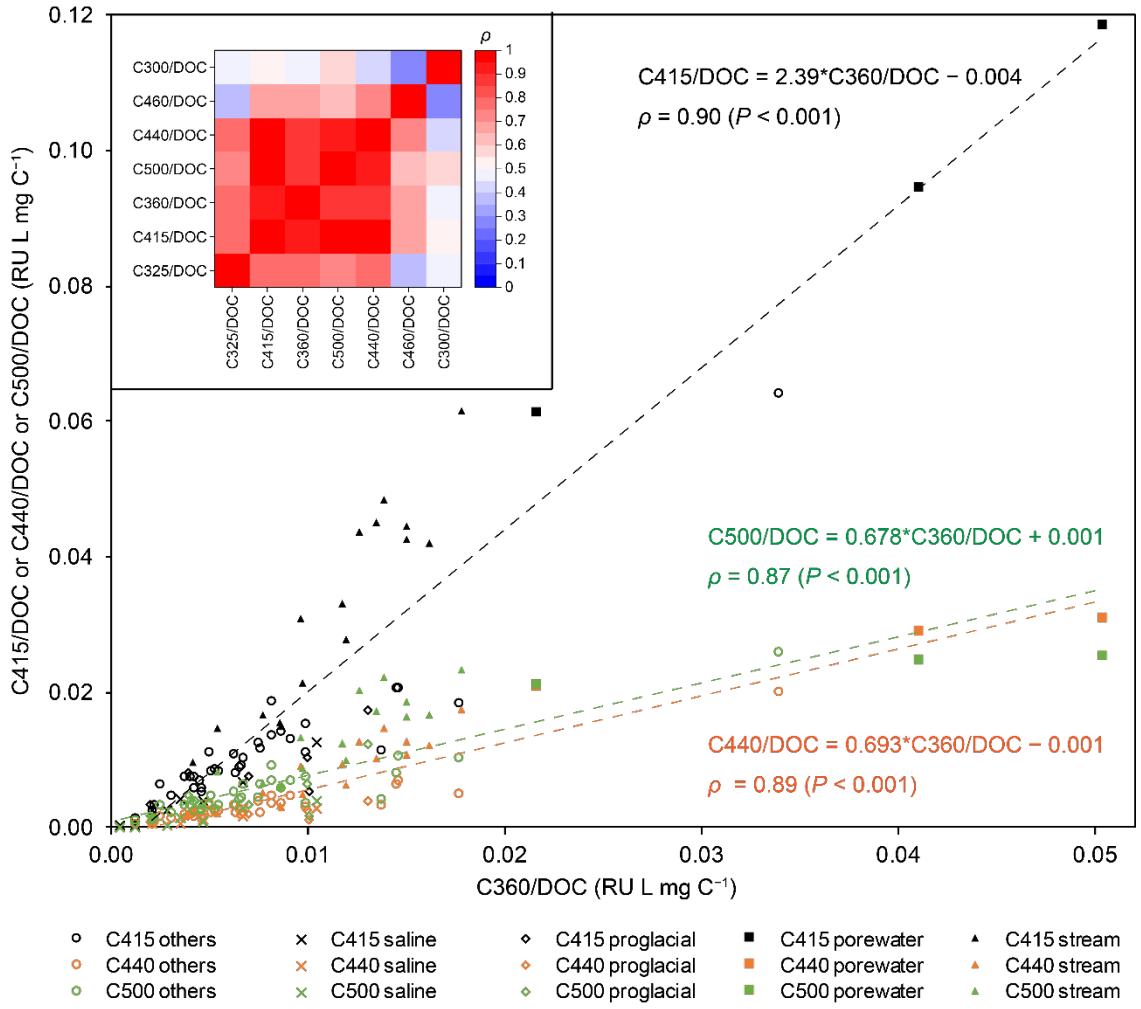
C415/DOC = 2.39*C360/DOC − 0.004
ρ = 0.90 (P < 0.001)
C500/DOC = 0.678*C360/DOC + 0.001
ρ = 0.87 (P < 0.001)
C440/DOC = 0.693*C360/DOC − 0.001
ρ = 0.89 (P < 0.001)
C415/DOC or C440/DOC or C500/DOC (RU L mg C⁻¹)
C360/DOC (RU L mg C⁻¹)
0.00
0.02
0.04
0.06
0.08
0.10
0.12
0.01
0.03
0.05
ρ
1
0.9
0.8
0.7
0.6
0.5
0.4
0.3
0.2
0.1
0
C300/DOC
C460/DOC
C440/DOC
C500/DOC
C360/DOC
C415/DOC
C325/DOC
C415 others
C440 others
C500 others
C415 saline
C440 saline
C500 saline
C415 proglacial
C440 proglacial
C500 proglacial
C415 porewater
C440 porewater
C500 porewater
C415 stream
C440 stream
C500 stream

Journal: Water Research

Supporting information for:

# Origin, distributions, and environmental significance of ubiquitous humic-like fluorophores in Antarctic lakes and streams

**Morimaru Kida[1†‡*], Taichi Kojima[1], Yukiko Tanabe[2, 3], Kentaro Hayashi[4], Sakae Kudoh[2, 3], Nagamitsu Maie[5], Nobuhide Fujitake[1]**

[1] Faculty of Agriculture, Graduate School of Agricultural Science, Kobe University, 1-1 Rokkodai, Nada, Kobe, Hyogo 657-8501, Japan

[2] National Institute of Polar Research, Research Organization of Information and Systems, 10-3 Midori-cho, Tachikawa, Tokyo 190-8518, Japan

[3] Department of Polar Science, SOKENDAI (The Graduate University for Advanced Studies), 10-3 Midori-cho, Tachikawa, Tokyo 190-8518, Japan

[4] Institute for Agro-Environmental Sciences, NARO, 3-1-3 Kannondai, Tsukuba, Ibaraki 305-8604, Japan

[5] School of Veterinary Medicine, Kitasato University, Towada, Aomori 034-8628, Japan

† Research Fellow of Japan Society for the Promotion of Science

‡ Present address: Research Group for Marine Geochemistry (ICBM-MPI Bridging Group), Carl von Ossietzky University of Oldenburg, Institute for Chemistry and Biology of the Marine Environment (ICBM), Carl-von-Ossietzky-Str. 9-11, 26129 Oldenburg, Germany

* corresponding author e-mail: morimaru.kida@people.kobe-u.ac.jp; Tell: +81-78-803-5846

ORCID ID: 0000-0002-9908-2012 (M.K.)

Contents; 4 tables, 10 figures

# Contents

Figure S1: Map and pictures

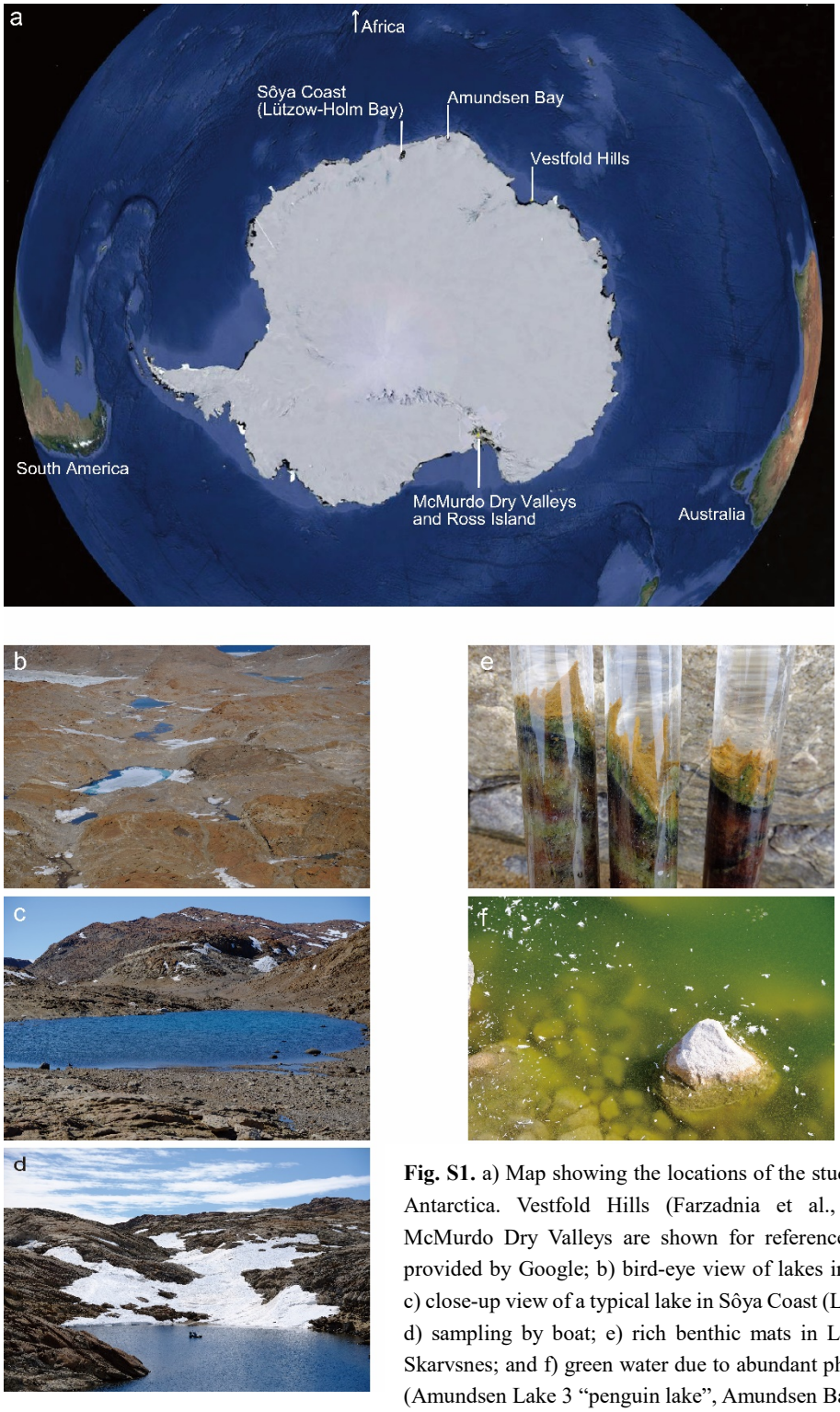


**Fig. S1.** a) Map showing the locations of the studied areas in Antarctica. Vestfold Hills (Farzadnia et al., 2017) and McMurdo Dry Valleys are shown for reference. Map data provided by Google; b) bird-eye view of lakes in Skarvsnes; c) close-up view of a typical lake in Sôya Coast (Lake Oyako); d) sampling by boat; e) rich benthic mats in Lake Hotoke, Skarvsnes; and f) green water due to abundant phytoplankton (Amundsen Lake 3 “penguin lake”, Amundsen Bay).

## SI 1. Optical index

We calculated optical indices from the absorbance and EEM data to estimate the structural properties and origin of DOM. Spectral slope ($S_{275–295}$), which has been related to apparent molecular weight (MW) and the degree of photodegradation (Helms et al., 2008) and used as a source differentiation (terrestrial vs marine) tool in estuarine studies (Fichot and Benner, 2012), was calculated using a linear fit to the natural log-transformed $a_\lambda$ spectrum in the ranges of 275–295 nm (coefficient of determination $R^2 > 0.97$; Fig. S3a). Typically, a higher (steeper) $S_{275–295}$ value suggests a decrease in molecular weight and aromaticity of DOM and an increase in the degree of photodegradation (Helms et al., 2008). DOC-specific ultraviolet absorbance ($SUVA_{254}$), which is related to aromaticity of humic substances (Weishaar et al., 2003) and can be used as a metric for %HPO (Kida et al., 2018) and the light absorbing ability of DOM, was calculated by dividing the UV absorbance ($m^{-1}$) measured at $\lambda$ = 254 nm by the DOC concentration (mg C $L^{-1}$). The lowest absorbance at 254 nm with a 5-cm path length cuvette (0.01) was sufficiently higher than the instrument measurement accuracy of 0.002 when the absorbance is < 0.5 (manufacturer provided).

The measurement locations of the fluorescent indices are provided in Fig. S5 for visualization purposes. The fluorescence index (FI) was calculated as the ratio of emission intensities at 470 and 520 nm ($I_{470}/I_{520}$) at 370 nm excitation (Cory et al. 2010). FI values are somewhat dependent on the instrument used even after instrument-specific response correction, and the FluoroMax gives the FI value of 1.42–1.55 for microbial end-member and 1.21 for soil end-member fulvic acids (Cawley et al., 2013; Cory et al., 2010). Four samples were found not to have humic fluorophores, and thus FI of these samples is not presented (Fig. S4). The biological index (BIX) was calculated as $I_{380}/I_{430}$ at 310 nm excitation and it estimates autochthonous biological production and subsequent heterotrophic consumption by bacteria in water environments. High values (> 1) of BIX correspond to DOM of predominantly autochthonous origin and to freshly released DOM in water, whereas lower values (0.6–0.7) correspond to low DOM production in natural waters (Huguet et al., 2009). The humification index (HIX) was calculated as the sum of $I_{435–480}$ divided by the sum of $I_{300–345} + I_{435–480}$ at 255 nm excitation and it ranges from 0 to 1 with increasing degrees of humification (Ohno, 2002).

## SI 2. PARAFAC

We analyzed the EEMs by parallel factor analysis (PARAFAC) to mathematically deconvolute them into distinct fluorescent components with independent spectral characteristics. The bottom water was collected at six lakes to increase the number of samples for PARAFAC, but their chemical properties are not discussed in this study because they were likely the mixture of the porewater and corresponding lake water. We used MATLAB R2017b with the *drEEM* toolbox (v 0.4.0) (Murphy et al., 2013). Despite the large fluorescence intensity differences among samples, EEMs were not normalized to total signals because normalization led to a worse and unstable model. During the exploratory phase, eight outliers were removed based on their leverage, and emission wavelengths below 318 nm were removed. PARAFAC was applied to the resulting EEM dataset (73 samples × 43 excitations × 117 emissions). The model was constrained to non-negative values. Models (5–7 components) were developed with a convergence criterion of $10^{-10}$. Each model was iterated 50 times after initializing with random starting values, and only the least squares solution was retained. The final seven-component model accounted for > 99.95% of the measured spectral variation and had a low core consistency value (0.48%). The appropriate component number was determined using residual analysis and external validation against published models (Murphy et al., 2018). Due to the limited number of samples (Murphy et al., 2013), split-half validation with random splitting did not produce a stable result (not always validated). The external validation was achieved by quantitatively comparing the identified fluorescent components with the published data using an open-access spectral database (OpenFluor; Murphy et al., 2014). On OpenFluor, one can compare fluorescence datasets and determine the Tucker congruence coefficient (TCC) between pairs of excitation ($TCC_{ex}$) and emission ($TCC_{em}$) spectra. If an identified fluorescent component has a strong match ($TCC_{ex \times em} > 0.95$), it means that the same and/or a spectrally indistinguishable validated component has been reported in the literature, and that the identified fluorescent component has legitimate spectral characteristics. The post-modeling residual analysis confirmed that the seven-component model adequately reproduced each EEM. This type of validation has been recently proposed for the one-sample PARAFAC approach (Murphy et al., 2018; Wünsch et al., 2017), and it was enabled here for the 'traditional' multi-sample PARAFAC owing to the open database. We note that a five-component model was also validated, but it often failed to adequately represent protein-like fluorescence and visible wavelength regions (Ex > 350 nm, Em > 400 nm). Also, three of the five identified components in the five-component model had much smaller (0–4) number of strong matches ($TCC_{ex \times em} > 0.95$) on OpenFluor, implying that the five-component model was not adequate. After model building, the outliers were projected onto the validated model to obtain scores for them. However, four out of the eight samples were not adequately modeled (judged by residuals); thus, their PARAFAC results are not presented.

# Table S1: Stream data

**Table S1.** The sampling locations and basic optical and chemical properties of DOM for samples collected from streams in Yukidori and Yatsude Valleys in Langhovde ice-free area.

| Stream name | Latitude (decimal) | Longitude (decimal) | Sampling date | Salinity | pH | Water temp. (°C) | DOC (mg C $L^{-1}$) | %HPO (%) | $a_{254}$ ($m^{-1}$) |
|---|---|---|---|---|---|---|---|---|---|
| Yukidori 1 | -69.24105 | 39.77995 | 8 Jan. 2017 | 0.022 | 8.59 | 1.2 | 0.326 | 38.0 | 0.79 |
| Yukidori 2 | -69.24072 | 39.77785 | 8 Jan. 2017 | 0.041 | 10.0 | 1.5 | 0.724 | 44.0 | 1.65 |
| Yukidori 3 | -69.24052 | 39.77172 | 8 Jan. 2017 | 0.038 | 8.59 | 2.5 | 0.664 | 38.7 | 1.40 |
| Yukidori 4 | -69.24057 | 39.76347 | 8 Jan. 2017 | 0.041 | 8.10 | 3.6 | 0.553 | 50.5 | 1.21 |
| Yukidori 6 | -69.24075 | 39.75300 | 11 Jan. 2017 | 0.037 | 7.08 | 8.3 | 0.850 | 37.7 | 0.82 |
| Yukidori 7 | -69.24090 | 39.74454 | 11 Jan. 2017 | 0.043 | 7.06 | 4.8 | 0.481 | 51.3 | 0.91 |
| Yukidori 8 | -69.24174 | 39.73134 | 11 Jan. 2017 | 0.049 | 7.06 | 7.9 | 0.525 | 40.2 | 1.29 |
| Yukidori 9 | -69.24226 | 39.71842 | 11 Jan. 2017 | 0.048 | 6.78 | 8.0 | 0.677 | 39.8 | 1.75 |
| Yatsude 1 | -69.26201 | 39.78727 | 9 Jan. 2017 | 0.052 | 7.20 | 1.8 | 0.436 | 40.0 | 0.89 |
| Yatsude 3 | -69.25331 | 39.76625 | 9 Jan. 2017 | 0.040 | 7.11 | 1.0 | 0.413 | 36.3 | 0.81 |
| Yatsude 4 | -69.25268 | 39.76462 | 9 Jan. 2017 | 0.047 | 7.17 | 0.9 | 0.460 | 41.6 | 1.07 |
| Yatsude 5 | -69.25173 | 39.76064 | 9 Jan. 2017 | 0.049 | 7.20 | 1.1 | 0.564 | 42.0 | 0.90 |
| Yatsude 6 | -69.24942 | 39.75051 | 9 Jan. 2017 | 0.046 | 7.03 | 2.2 | 0.707 | 26.9 | 1.26 |
| Yatsude 7 | -69.24752 | 39.74376 | 9 Jan. 2017 | 0.048 | 6.93 | 2.1 | 0.690 | 29.1 | 1.30 |
| Yatsude 8 | -69.24531 | 39.73379 | 9 Jan. 2017 | 0.038 | 7.07 | 5.0 | 0.320 | 47.6 | 0.70 |
| Yatsude 9 | -69.24416 | 39.71998 | 16 Jan. 2017 | 0.058 | 7.13 | 3.0 | 0.643 | 60.5 | 0.69 |

Yukidori 5 = Lake Yukidori, Yatsude 2 = Lake Heito (See Table 1).

Figure S2: Water chemistry depth profile of the sampled lakes

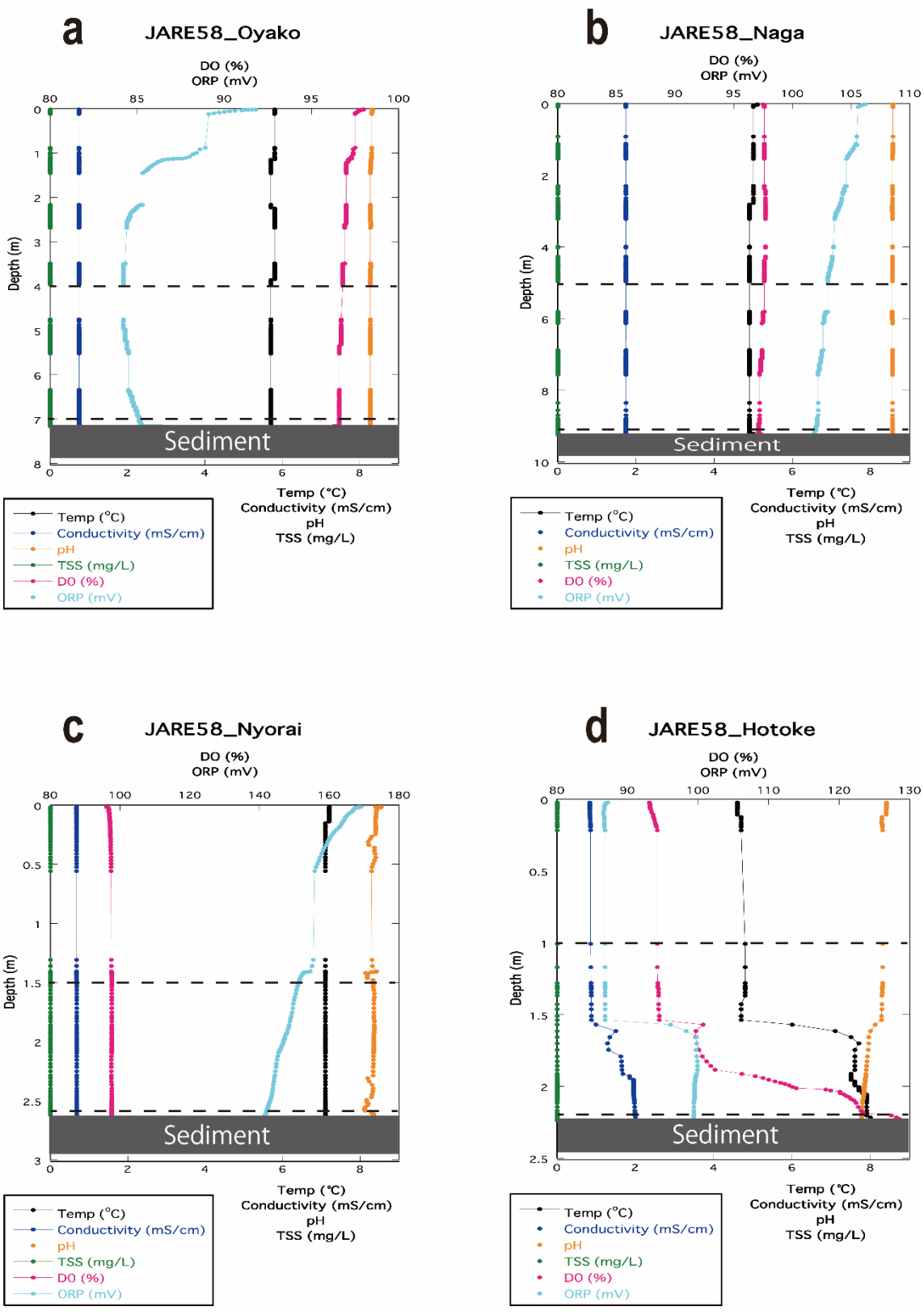

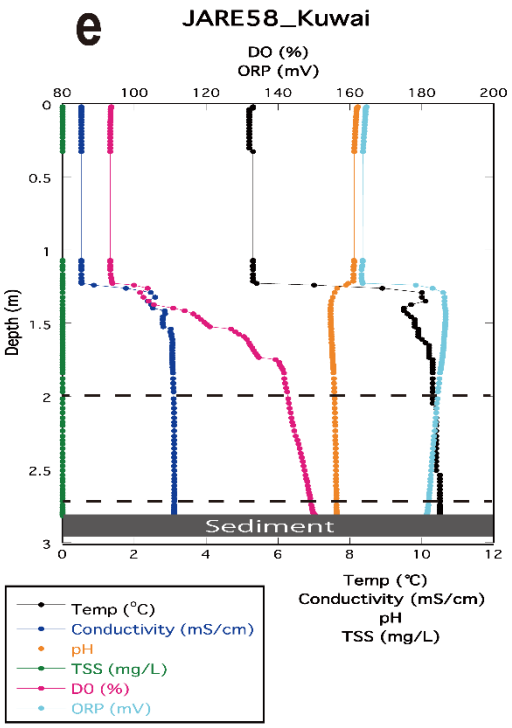
e
JARE58_Kuwai
DO (%)
ORP (mV)
Depth (m)
Sediment
Temp (℃)
Conductivity (mS/cm)
pH
TSS (mg/L)
Temp (°C)
Conductivity (mS/cm)
pH
TSS (mg/L)
DO (%)
ORP (mV)

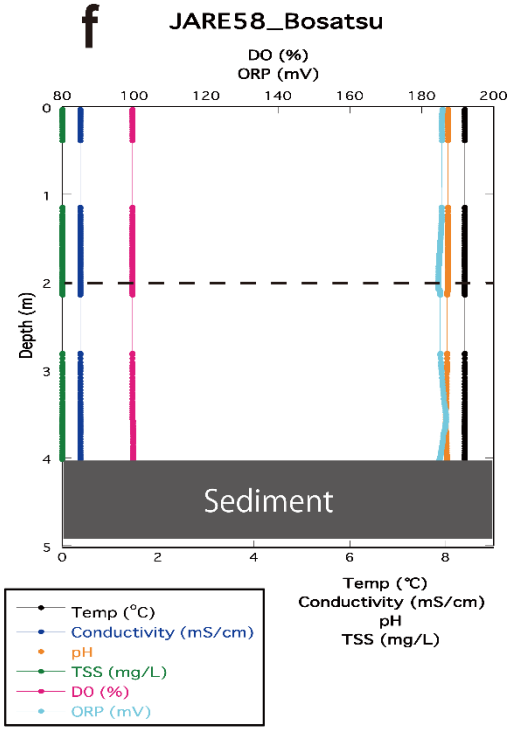
f
JARE58_Bosatsu
DO (%)
ORP (mV)
Depth (m)
Sediment
Temp (℃)
Conductivity (mS/cm)
pH
TSS (mg/L)
Temp (°C)
Conductivity (mS/cm)
pH
TSS (mg/L)
DO (%)
ORP (mV)

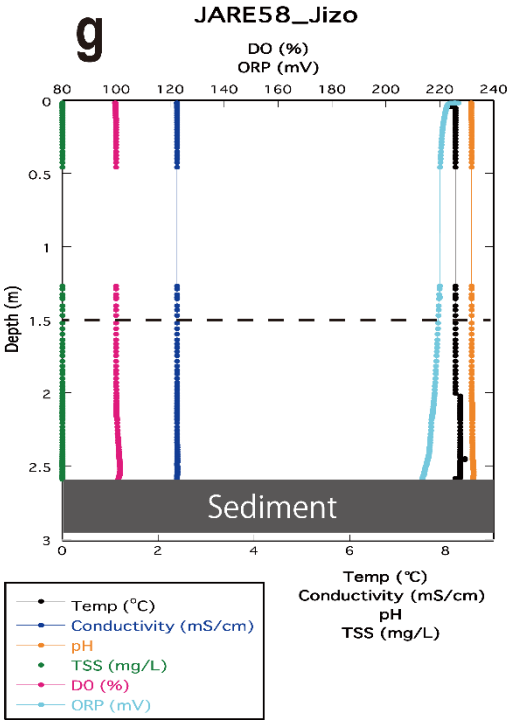
g
JARE58_Jizo
DO (%)
ORP (mV)
Depth (m)
Sediment
Temp (℃)
Conductivity (mS/cm)
pH
TSS (mg/L)
Temp (°C)
Conductivity (mS/cm)
pH
TSS (mg/L)
DO (%)
ORP (mV)

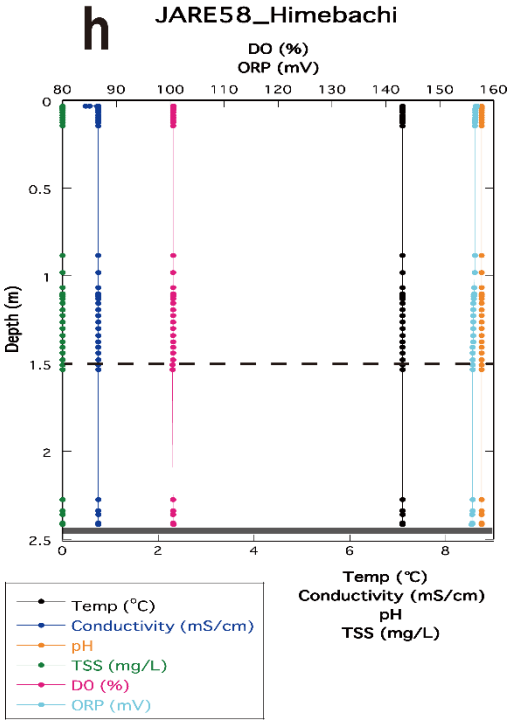
h
JARE58_Himebachi
DO (%)
ORP (mV)
Depth (m)
Temp (℃)
Conductivity (mS/cm)
pH
TSS (mg/L)
Temp (°C)
Conductivity (mS/cm)
pH
TSS (mg/L)
DO (%)
ORP (mV)

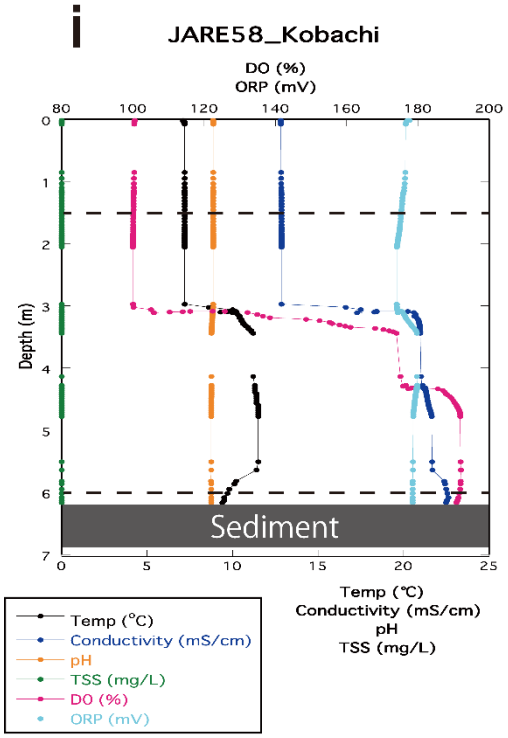
i
JARE58_Kobachi
DO (%)
ORP (mV)
Depth (m)
Sediment
Temp (℃)
Conductivity (mS/cm)
pH
TSS (mg/L)
Temp (°C)
Conductivity (mS/cm)
pH
TSS (mg/L)
DO (%)
ORP (mV)

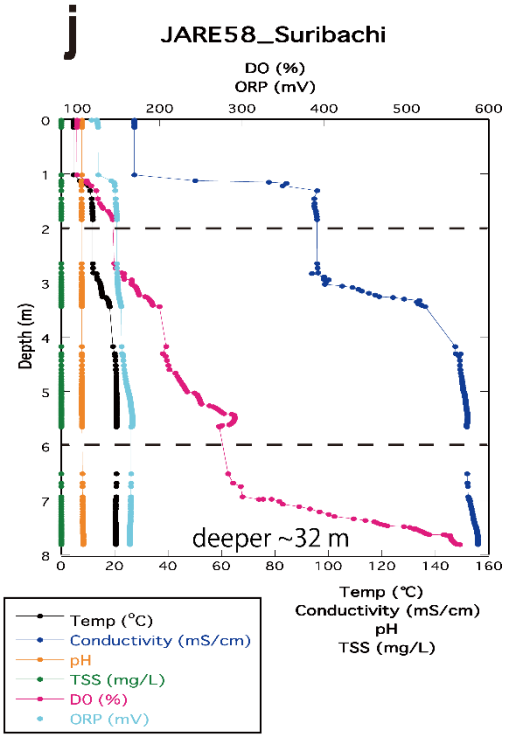
j
JARE58_Suribachi
DO (%)
ORP (mV)
Depth (m)
deeper ~32 m
Temp (℃)
Conductivity (mS/cm)
pH
TSS (mg/L)
Temp (°C)
Conductivity (mS/cm)
pH
TSS (mg/L)
DO (%)
ORP (mV)

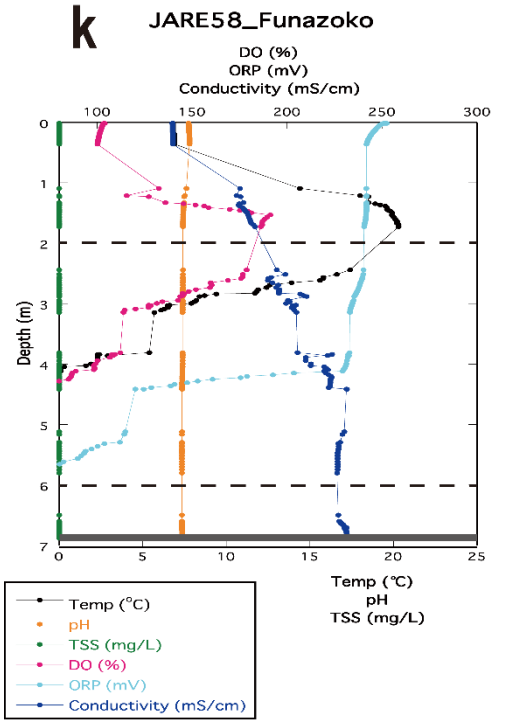
k
JARE58_Funazoko
DO (%)
ORP (mV)
Conductivity (mS/cm)
Depth (m)
Temp (℃)
pH
TSS (mg/L)
Temp (°C)
pH
TSS (mg/L)
DO (%)
ORP (mV)
Conductivity (mS/cm)

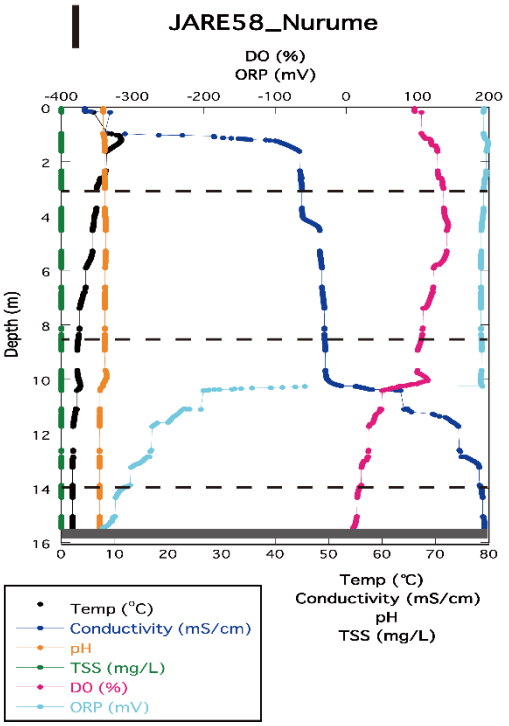
l
JARE58_Nurume
DO (%)
ORP (mV)
Depth (m)
Temp (℃)
Conductivity (mS/cm)
pH
TSS (mg/L)
Temp (°C)
Conductivity (mS/cm)
pH
TSS (mg/L)
DO (%)
ORP (mV)

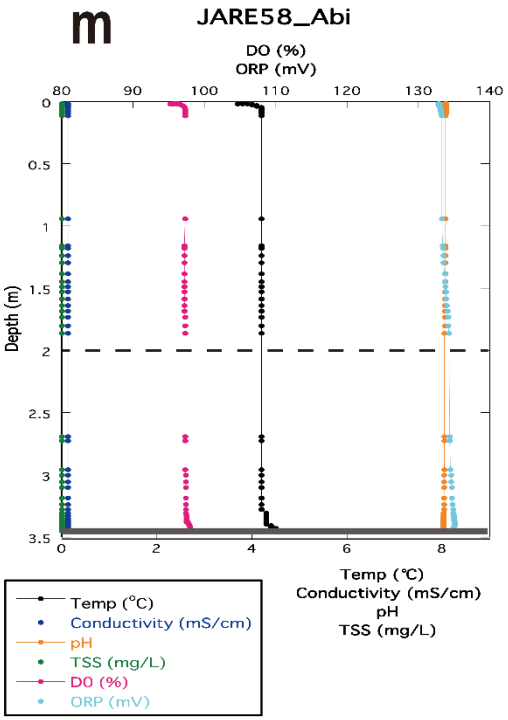
m
JARE58_Abi
DO (%)
ORP (mV)
Depth (m)
Temp (℃)
Conductivity (mS/cm)
pH
TSS (mg/L)
Temp (°C)
Conductivity (mS/cm)
pH
TSS (mg/L)
DO (%)
ORP (mV)

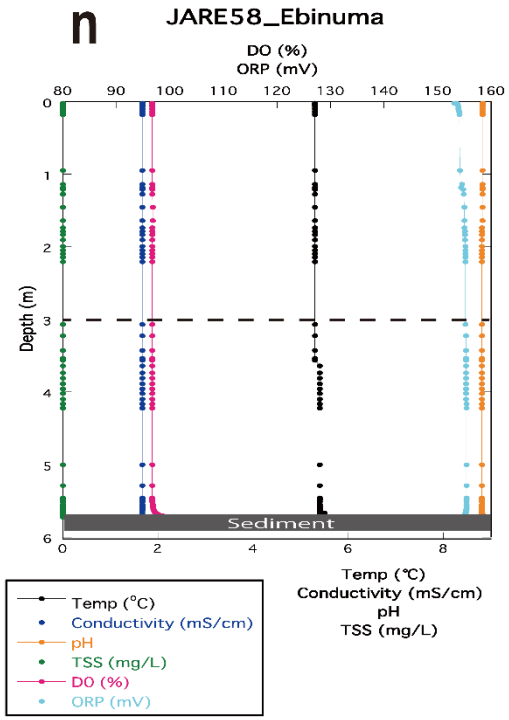
n
JARE58_Ebinuma
DO (%)
ORP (mV)
Depth (m)
Sediment
Temp (℃)
Conductivity (mS/cm)
pH
TSS (mg/L)
Temp (°C)
Conductivity (mS/cm)
pH
TSS (mg/L)
DO (%)
ORP (mV)

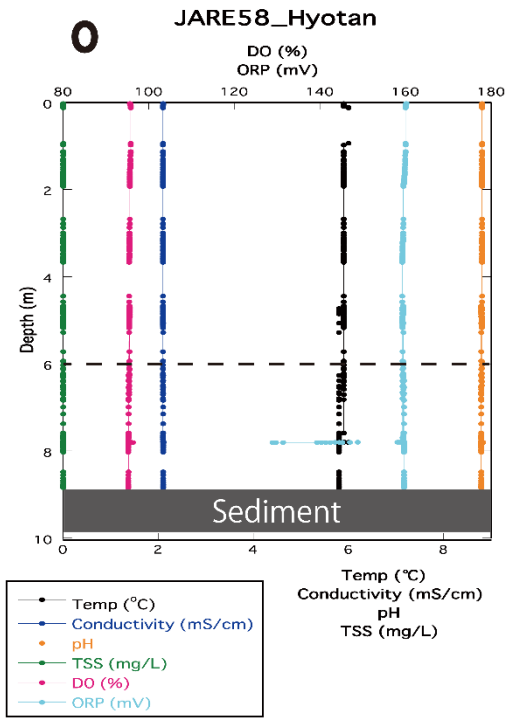
o
JARE58_Hyotan
DO (%)
ORP (mV)
Depth (m)
Sediment
Temp (℃)
Conductivity (mS/cm)
pH
TSS (mg/L)
Temp (°C)
Conductivity (mS/cm)
pH
TSS (mg/L)
DO (%)
ORP (mV)

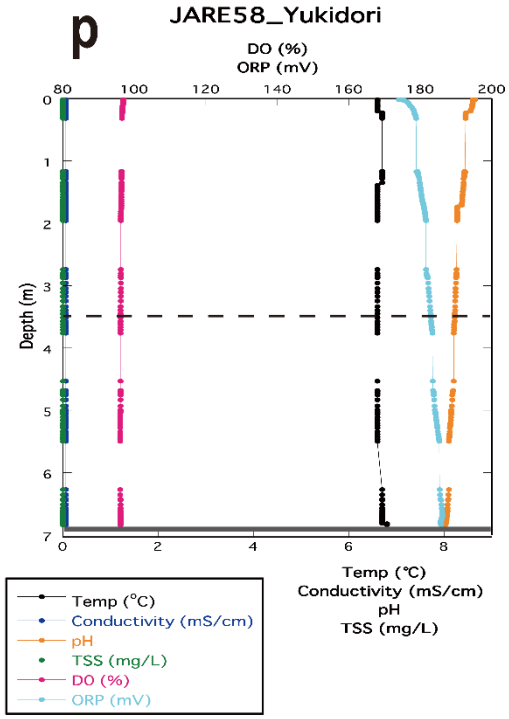
p
JARE58_Yukidori
DO (%)
ORP (mV)
Depth (m)
Temp (℃)
Conductivity (mS/cm)
pH
TSS (mg/L)
Temp (°C)
Conductivity (mS/cm)
pH
TSS (mg/L)
DO (%)
ORP (mV)

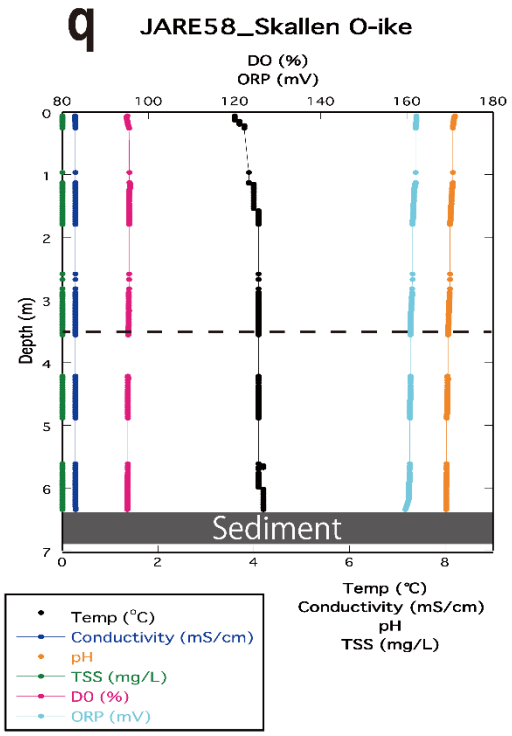


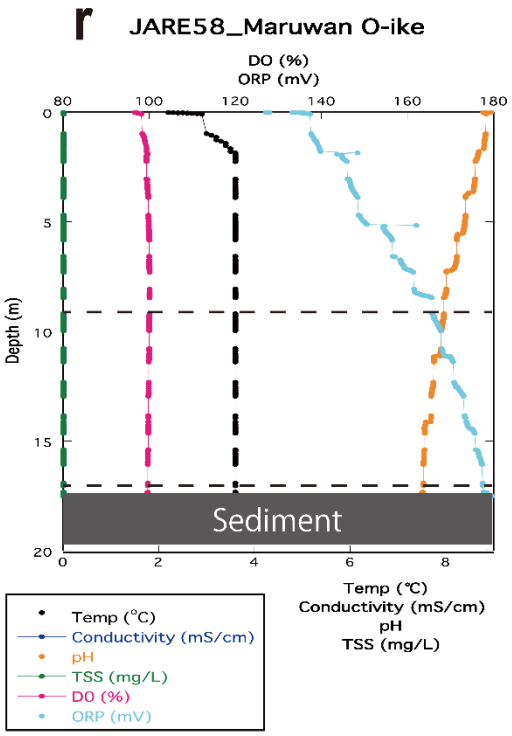


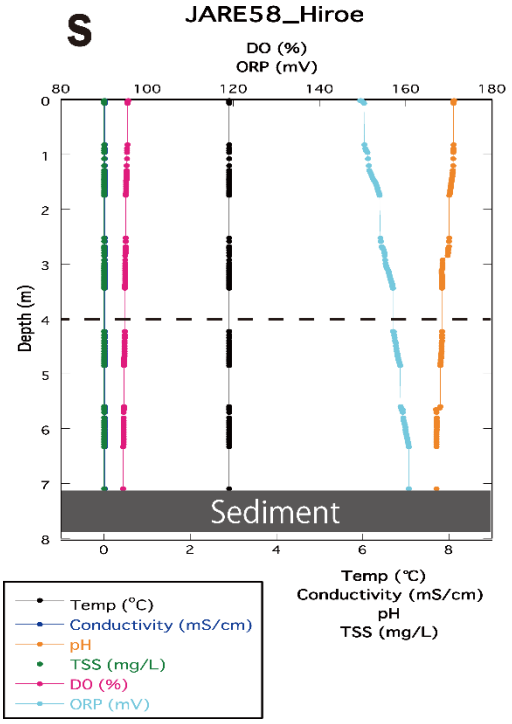


**Fig. S2 (a–s).** Water chemistry depth profile of the sampled lakes during the 58th Japanese Antarctic Research Expedition (JARE58). DO = dissolved oxygen. TSS = total suspended solid. ORP = oxidation-reduction potential. Electric conductivity values are presented as a 25°C equivalent. Water chemistry was measured using a multi-water quality logger (YSI 6600 V2, YSI Inc.) at the time of sampling at the deepest point of the lakes. Horizontal dashed lines indicate the sampling depth. Saline lakes (i–l) have a clear water stratification, while that of Hotoke (d) and Kuwai (e) was due to the melt water inflow.

Figure S3: Quality assurance for the $S_{275–295}$ and %HPO determination

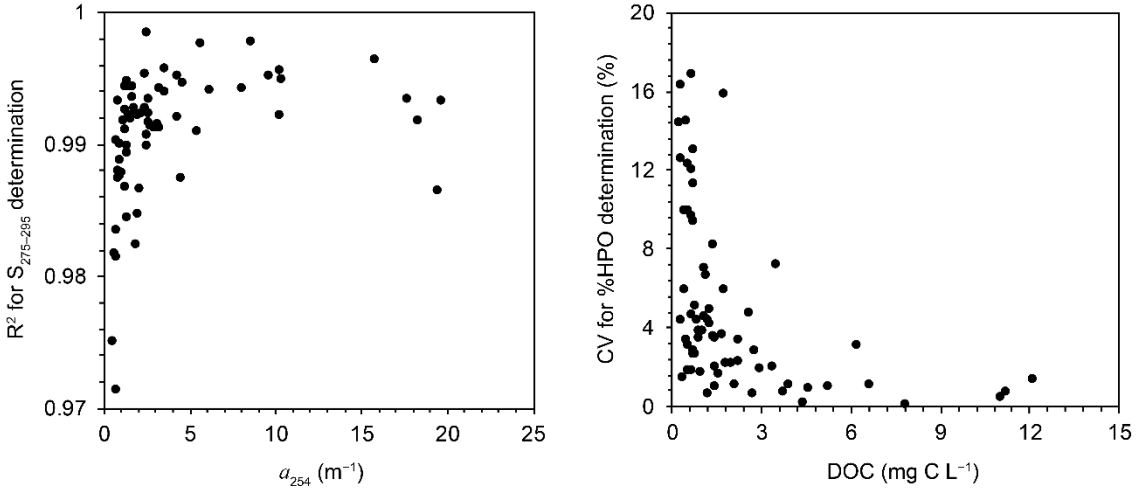


**Fig. S3.** Quality assurance. Coefficient of determination ($R^2$) for the $S_{275–295}$ determination by linear regression of natural log-transformed *a* spectra as a function of $a_{254}$ and coefficient of variation (CV) of the quadruplicate determination of the proportion of hydrophobic fraction (HPO) of DOM by the DAX-8 batch adsorption as a function of DOC.

Figure S4: Samples without humic fluorophores

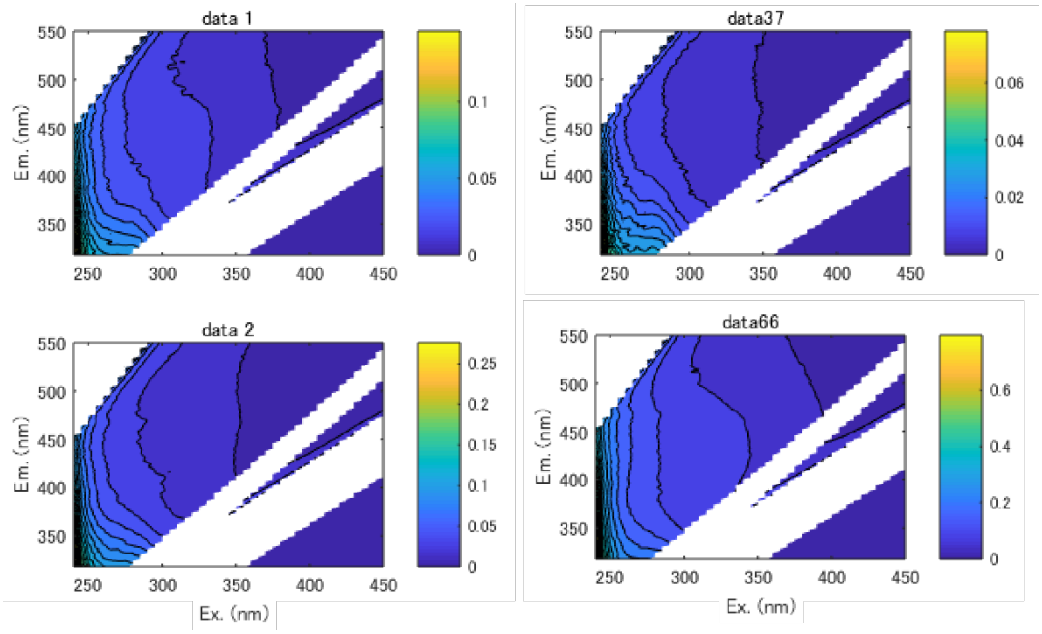


**Fig. S4.** Samples without humic fluorophores. Fluorescence index (FI) of these samples is not presented since FI = ~1 and meaningless due to the absence of fluorescence in the region where FI is calculated (Ex = 370 nm). Also, the established PARAFAC model could not adequately represent EEMs of these samples, so their PARAFAC results are not presented. The samples are: glacial lake (data 1) and glacial water (data 2) in Skarvsnes, Maruwan-Oike in Rundvågshetta (data 37), and Amundsen Lake1 (data 66) in Amundsen Bay.

Figure S5: Measurement locations of FDOM indices

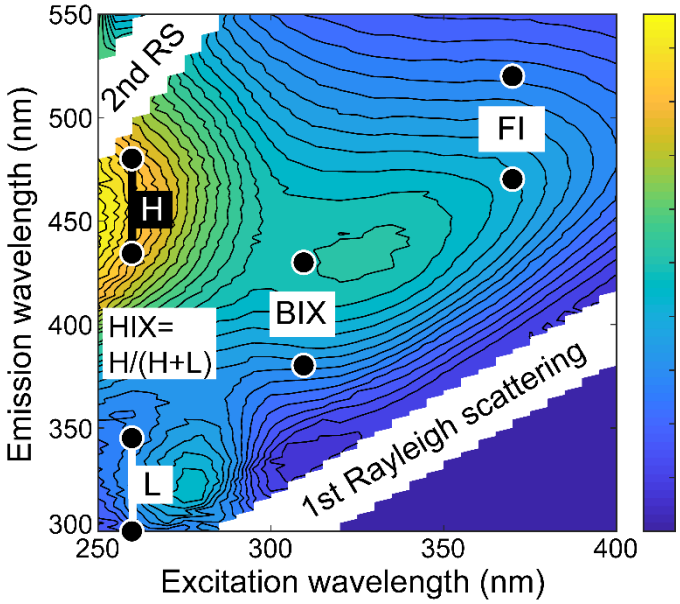


**Fig. S5.** Excitation emission matrix and measurement locations of fluorescent indices. Fluorescent intensity is presented in color (arbitrary unit). The two points used in the fluorescence index (FI, $I_{470}/I_{520}$) and biological index (BIX, $I_{380}/I_{430}$) are represented by filled circles at an excitation of 370 nm and 310 nm, respectively. The humification index (HIX) is calculated by area under an emission of 435–480 nm (H) divided by area under an emission of 435–480 nm (H) + 300–345 nm (L) at an excitation of 254 nm. In this study, HIX was calculated at an excitation of 255 nm.

# Table S2: Nutrient data

**Table S2.** Nutrients concentrations of the studied lakes and streams. Blank cells indicate that nutrients concentrations were below the detection limit of the analyzer. See Table 1 for the detailed information of lakes.

| Area name | Lake/stream name | Depth | Salinity | $NO_2^-$ µmol/L | $NO_3^-$ µmol/L | $NH_4^+$ µmol/L | %DON | $PO_4^{3-}$ µmol/L | $SiO_3^{2-}$ µmol/L |
|---|---|---|---|---|---|---|---|---|---|
| Amundsen | Amundsen Lake1 | shore | 0.04 | 0.08 | 18.23 | 1.08 | 44.0 | 4.35 | 73.17 |
| Amundsen | Amundsen Lake2 | shore | 0.03 | | | 0.59 | 97.8 | 0.41 | 3.29 |
| Amundsen | Amundsen Lake3 | shore | 0.19 | 3.82 | 276.34 | 11.94 | 29.3 | 31.70 | 173.49 |
| Amundsen | Richardson | shore | 0.02 | | Tr | 0.35 | 98.5 | 3.17 | 7.77 |
| Breivågnipa | Hiroe | 4 m | 0.02 | | | | 100 | | 2.60 |
| Breivågnipa | Breivagnipa Lake1 | shore | 0.20 | | | 0.44 | 98.4 | | 97.09 |
| Langhovde | Yukidori (Yukidori 5) | 3.5 m | 0.03 | | 2.33 | 0.27 | 75.6 | Tr | 16.17 |
| Langhovde | Yukidori (Yukidori 5) | pore | 0.31 | NA | NA | NA | NA | NA | NA |
| Langhovde | Mitsuike Ue | shore | 0.61 | Tr | 5.20 | 0.42 | 80.4 | | 129.53 |
| Langhovde | Mitsuike Naka | shore | 0.79 | Tr | 3.19 | 0.25 | 83.2 | | 204.53 |
| Langhovde | Mitsuike Shita | shore | 0.88 | Tr | 4.88 | 0.82 | 81.0 | | 159.57 |
| Langhovde | Nurume | 3 m | 29.11 | | | 0.17 | 99.2 | 0.24 | 6.01 |
| Langhovde | Nurume | 8.5 m | 32.20 | Tr | | 3.49 | 92.9 | 0.98 | 8.61 |
| Langhovde | Nurume | 14 m | 54.73 | 0.08 | 1.22 | 479.10 | NA | 45.63 | 119.44 |
| Langhovde | Heito (Yatsude 2) | shore | 0.02 | 0.20 | 3.38 | 0.17 | 76.3 | | 4.50 |
| Rundvågshetta | Maruwan-Oike | 9 m | 0.02 | | | 0.06 | 99.4 | | 2.56 |
| Rundvågshetta | Maruwan Kita | shore | 0.02 | | Tr | 0.43 | 97.2 | | 2.96 |
| Rundvågshetta | Maruwan Minami | shore | 0.02 | | | 0.09 | 99.2 | | 14.93 |
| Skallen | Skallen-Oike | 3.5 m | 0.13 | | | 0.20 | 98.4 | | 73.86 |
| Skallen | Skallen-Oike | pore | 0.14 | NA | NA | NA | NA | NA | NA |
| Skallen | Skallen Lake1 | shore | 0.07 | | | 0.17 | 98.2 | | 30.08 |
| Skallen | Skallen Lake2 | shore | 0.05 | | Tr | Tr | 96.0 | | 39.04 |
| Skallen | Skallen Lake3 | shore | 0.08 | | | 0.16 | 98.9 | | 52.10 |
| Skallen | Skallen Lake4 | shore | 0.04 | | | Tr | 99.5 | | 28.10 |
| Skallen | Skallen Lake5 | shore | 0.03 | | | Tr | 98.9 | | 15.95 |
| Skallen | Glacial Lake | shore | 0.07 | | | Tr | 99.8 | Tr | 12.69 |
| Skallen | Glacial Water | stream | 0.02 | | Tr | 0.57 | 83.5 | 0.34 | Tr |
| Skarvsnes | Oyako | 4 m | 0.36 | NA | NA | NA | NA | NA | NA |
| Skarvsnes | Naga | 5 m | 0.88 | | | Tr | 100 | | 91.26 |
| Skarvsnes | Naga | pore | 0.88 | NA | NA | NA | NA | NA | NA |
| Skarvsnes | Nyorai | 1.5 m | 0.33 | | | Tr | 99.9 | | 102.01 |
| Skarvsnes | Nyorai | pore | 0.33 | NA | NA | NA | NA | NA | NA |
| Skarvsnes | Hotoke | 1 m | 0.42 | | | Tr | 99.4 | | 87.62 |
| Skarvsnes | Hotoke | pore | 1.02 | NA | NA | NA | NA | NA | NA |
| Skarvsnes | Kuwai | 2 m | 1.61 | | | 0.16 | 98.0 | | 69.13 |

**Table S2.** Continued.

| Area name | Lake/stream name | Depth | Salinity | $NO_2^-$ µmol/L | $NO_3^-$ µmol/L | $NH_4^+$ µmol/L | %DON | $PO_4^{2-}$ µmol/L | $SiO_3^{2-}$ µmol/L |
|---|---|---|---|---|---|---|---|---|---|
| Skarvsnes | Bosatsu | 2 m | 0.18 | | | 0.17 | 99.7 | | 61.17 |
| Skarvsnes | Jizo | 1.5 m | 1.23 | | | Tr | 99.9 | | 116.50 |
| Skarvsnes | Himago | shore | 3.90 | | | 0.15 | 99.6 | Tr | 21.46 |
| Skarvsnes | Mago | shore | 2.23 | | | 0.13 | 99.7 | | 19.81 |
| Skarvsnes | Sara | 1.5 m | 0.37 | | | Tr | 99.8 | | 93.61 |
| Skarvsnes | Tokkuri | shore | 0.87 | | | 0.18 | 99.6 | | 47.84 |
| Skarvsnes | Kumogata | shore | 0.65 | | | 0.60 | 98.2 | | 74.74 |
| Skarvsnes | Hyotan | 6 m | 1.07 | | | Tr | 100 | | 11.55 |
| Skarvsnes | Hamagiku | 2 m | 0.06 | | | 0.17 | 99.1 | | 63.04 |
| Skarvsnes | Ebi | 3 m | 0.84 | | Tr | Tr | 99.4 | | 71.51 |
| Skarvsnes | Kikuno | shore | 1.23 | | | Tr | 99.8 | | 123.48 |
| Skarvsnes | Hashioki | shore | 0.27 | | | Tr | 99.8 | | 171.60 |
| Skarvsnes | Skarvsnes Lake2 | shore | 0.96 | | Tr | Tr | 99.7 | | 66.56 |
| Skarvsnes | A-5 | shore | 0.39 | | 0.57 | 0.78 | 96.5 | | 207.49 |
| Skarvsnes | Hechima | shore | 1.67 | | Tr | Tr | 98.9 | | 169.75 |
| Skarvsnes | Magobachi | shore | 1.02 | | 0.80 | Tr | 95.7 | | 95.15 |
| Skarvsnes | Misumi | shore | 0.09 | | Tr | Tr | 97.1 | | 58.60 |
| Skarvsnes | Kobachi | 1.5 m | 7.37 | | | 0.14 | 99.6 | Tr | 36.32 |
| Skarvsnes | Kobachi | 6 m | 13.59 | | | Tr | 99.8 | 0.06 | 46.49 |
| Skarvsnes | Suribachi | 2 m | 69.84 | | | 6.58 | 93.4 | | 65.67 |
| Skarvsnes | Suribachi | 6 m | 121.35 | | | 4.58 | 97.8 | 0.64 | 151.70 |
| Skarvsnes | Funazoko | 2 m | 154.99 | | | 153.20 | 80.7 | | 131.93 |
| Skarvsnes | Funazoko | 6 m | 179.40 | | 5.66 | 288.14 | 75.9 | 0.41 | 162.02 |
| Langhovde | Yukidori 1 | stream | 0.02 | 0.57 | 12.18 | 0.22 | 28.2 | | 6.16 |
| Langhovde | Yukidori 2 | stream | 0.04 | 1.54 | 57.82 | 0.21 | 10.4 | Tr | 26.52 |
| Langhovde | Yukidori 3 | stream | 0.04 | 1.00 | 57.53 | 0.18 | 11.4 | | 19.62 |
| Langhovde | Yukidori 4 | stream | 0.04 | 0.59 | 57.94 | 0.19 | 8.7 | Tr | 17.50 |
| Langhovde | Yukidori 6 | stream | 0.04 | Tr | 3.06 | 0.15 | 72.9 | Tr | 23.70 |
| Langhovde | Yukidori 7 | stream | 0.04 | | 21.29 | 0.16 | 28.2 | Tr | 27.29 |
| Langhovde | Yukidori 8 | stream | 0.05 | Tr | 26.31 | 0.16 | 27.4 | | 42.12 |
| Langhovde | Yukidori 9 | stream | 0.05 | 0.15 | 23.36 | 0.31 | 30.7 | | 34.38 |
| Langhovde | Yatsude 1 | stream | 0.05 | 0.13 | 5.96 | 0.14 | 40.8 | | 50.30 |
| Langhovde | Yatsude 3 | stream | 0.04 | 0.21 | 1.38 | | 79.9 | | 15.99 |
| Langhovde | Yatsude 4 | stream | 0.05 | 0.25 | 16.62 | 0.18 | 22.9 | Tr | 17.79 |
| Langhovde | Yatsude 5 | stream | 0.05 | 0.08 | 19.05 | 0.31 | 28.2 | Tr | 19.11 |
| Langhovde | Yatsude 6 | stream | 0.05 | Tr | 44.26 | 0.14 | 21.5 | 0.07 | 19.37 |
| Langhovde | Yatsude 7 | stream | 0.05 | 0.17 | 53.85 | 0.13 | 15.2 | Tr | 18.85 |
| Langhovde | Yatsude 8 | stream | 0.04 | 0.08 | 40.22 | Tr | 18.5 | Tr | 11.95 |
| Langhovde | Yatsude 9 | stream | 0.06 | Tr | 40.82 | Tr | 21.3 | | 40.76 |

NA, not analyzed; Tr, below the quantification limit and thus values not shown

Figure S6: Distribution of FI, BIX, and HIX along salinity

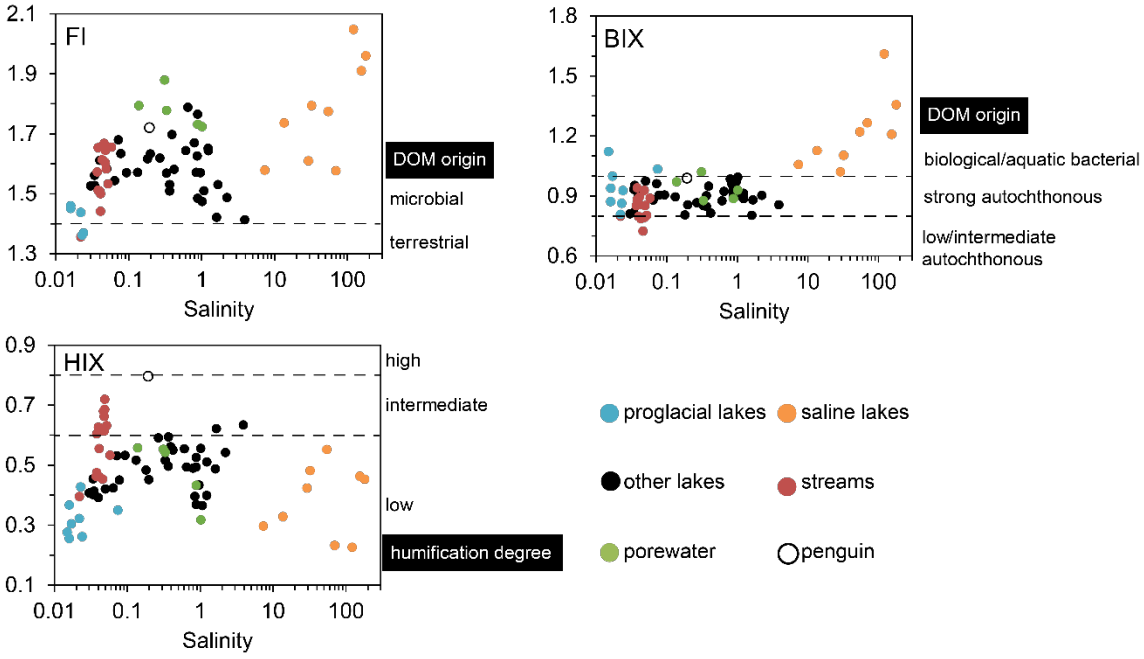


**Fig. S6.** Distribution of fluorescence index (FI), biological index (BIX), and humification index (HIX) along salinity. Samples are color-coded according to the sampling category, and 'penguin' lake is a turbid, green-colored lake with abundant phytoplankton because of penguin guano inputs from nearby colonies (Amundsen Lake3, Fig. S1f). The interpretation of index values is presented on the right side of each figure along with the threshold lines to decide DOM origin and property (Cory et al., 2010; Cory and McKnight, 2005; Huguet et al., 2009; Ohno, 2002). FI and BIX values of saline lake samples were high. HIX values of stream samples and Amundsen Lake 3 were higher than those of others at the corresponding salinity.

# Table S3: Assignments of the identified PARAFAC components

**Table S3.** Assignments of the identified PARAFAC components with the criterion of Tucker congruence coefficient ($TCC_{ex\times em}$) >0.95 using OpenFluor database. Red color indicates that an identified fluorescent component has $TCC_{ex\times em}$ between 0.9 and 0.95, which is a fair threshold that takes into account variability that can arise from modeling and comparing two completely independent datasets (Lorenzo-Seva and ten Berge, 2006; Wünsch et al., 2017)..

| | Source | Data name | Comp No. | Description | References |
|---|---|---|---|---|---|
| **C1** | Autochthonous | IPY-C3O | C4 | protein-like | (Guéguen et al., 2014) |
| **(C325)** | | Kattegat | C6 | tryptophan-like | (Osburn and Stedmon, 2011) |
| | Allochthonous | Not found | | | |
| | Ubiquitous | Not found | | | |
| **C2** | Autochthonous | TropicalRivers | C3 | microbial humic-like | (Yamashita et al., 2010a) |
| **(C415)** | | DarkOcean | C2 | in situ microbial production of fluorescent humic-like materials | (Catalá et al., 2015) |
| | Allochthonous | DaecheongReservoir | C2 | terrestrially derived humic substances | (Li et al., 2016) |
| | | LiverpoolBay | C1 | terrestrial humic-like | (Yamashita et al., 2011) |
| | Ubiquitous | Pantanal3_ww | C1 | ubiquitous | (Murphy et al., 2018) |
| | | Partners | C1 | ubiquitous in aquatic environments | (Walker et al., 2013) |
| **C3** | Autochthonous | DW_Sweden_Gavle | C4 | tryptophan-like | (Heibati et al., 2017) |
| **(C360)** | | horsens2003 | C5 | combination of peaks N and T | (Stedmon et al., 2003) |
| | Allochthonous | Beringia | C4 | not been reported previously/humic-like | (Walker et al., 2009) |
| | Ubiquitous | Not found | | | |

**Table S3.** Continued

| | Source | Data name | Comp No. | Description | References |
|---|---|---|---|---|---|
| **C4** | Autochthonous | Not found | | | |
| **(C500)** | Allochthonous | BalticIce | C2 | terrestrially derived humic | (Stedmon et al., 2007) |
| | | CoastalBEPOM | C2 | terrestrial humic | (Brym et al., 2014) |
| | Ubiquitous | osPARAFAC_PonyLake | C6 | one-sample decomposition of FDOM from Pony Lake | (Wünsch et al., 2017) |
| | | Pantanal3_ww | C3 | ubiquitous | (Murphy et al., 2018) |
| | | Horsens2005 | C2 | fulvic acid fluorophore group. Present in all environments | (Stedmon and Markager, 2005a) |
| **C5** | Autochthonous | LiverpoolBay | C2 | not defined by Coble et al/microbial humic-like | (Yamashita et al., 2011) |
| **(C440)** | | TropicalRivers | C4 | not defined by Coble et al/microbial humic-like | (Yamashita et al., 2010a) |
| | Allochthonous | Kattegat | C3 | terrestrial humic A peak | (Osburn and Stedmon, 2011) |
| | | Kauai | C8 | Terrestrial humic substances A and C peak | (Murphy et al., 2008) |
| | Ubiquitous | GoMaine | C7 | ubiquitous humic-like | (Cawley et al., 2012) |
| | | Horsens2005 | C4 | fulvic acid fluorophore group. Present in all environments | (Stedmon and Markager, 2005a) |
| **C6**† | Autochthonous | Bergen | C1 | microbial processing of algae-derived DOM | (Stedmon and Markager, 2005b) |
| **(C460)** | Allochthonous | Horsens2005 | C1 | terrestrial humic fluorophore group, photodegradation restricted to UVB and UVC | (Stedmon and Markager, 2005a) |
| | | FCE | C2 | terrestrial humic-like, suggested as photo-refractory | (Yamashita et al., 2010b) |
| | Ubiquitous | Not found | | | |
| **C7** | Autochthonous | RecycleStM | G4 | tyrosine-like | (Murphy et al., 2011) |
| **(C300)** | | DarkOcean | C4 | tyrosine-like | (Catalá et al., 2015) |
| | | BalticIce | C5 | tryptophan associated with proteins | (Stedmon et al., 2007) |
| | Allochthonous | Not found | | | |
| | Ubiquitous | Not found | | | |

† A UVC humic-like component is often reported as accounting for the largest variability in the dataset, while $C_{460}$ had the second smallest explaining variability in this study. This may be because environments with a large contribution from terrestrial sources are often largely affected by a UVC humic-like component, while the Antarctic lakes and streams had little, if any, terrestrial inputs (such as aerial dusts).

Figure S7: PARAFAC comparisons with ubiquitous models

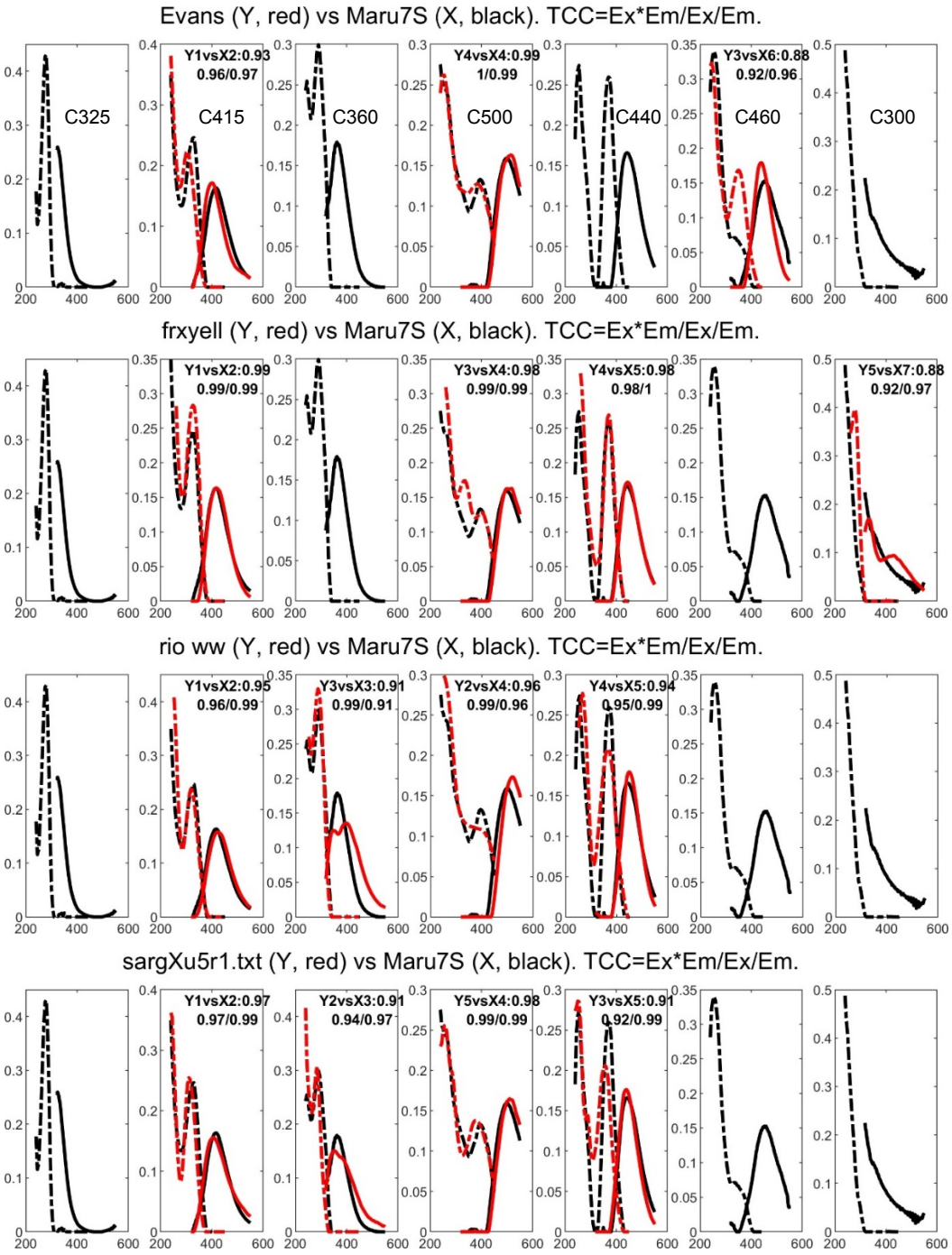


**Fig. S7.** Comparisons of our PARAFAC model with PARAFAC models from the "ubiquity" paper (Murphy et al., 2018). Our 7-component model is shown in black, while 4- or 5-compoennt ubiquity models are in red. Pretty good matches are found for e.g. two Antarctic samples (coastal sample of Cape Evans and Lake Fryxell), Rio Negro (Brazil), and the deep Sargasso Sea (4534 m), especially for $C_{415}$, $C_{500}$, and $C_{440}$ which we considered as ubiquitous components.

Figure S8: Distribution of the identified PARAFAC components along salinity

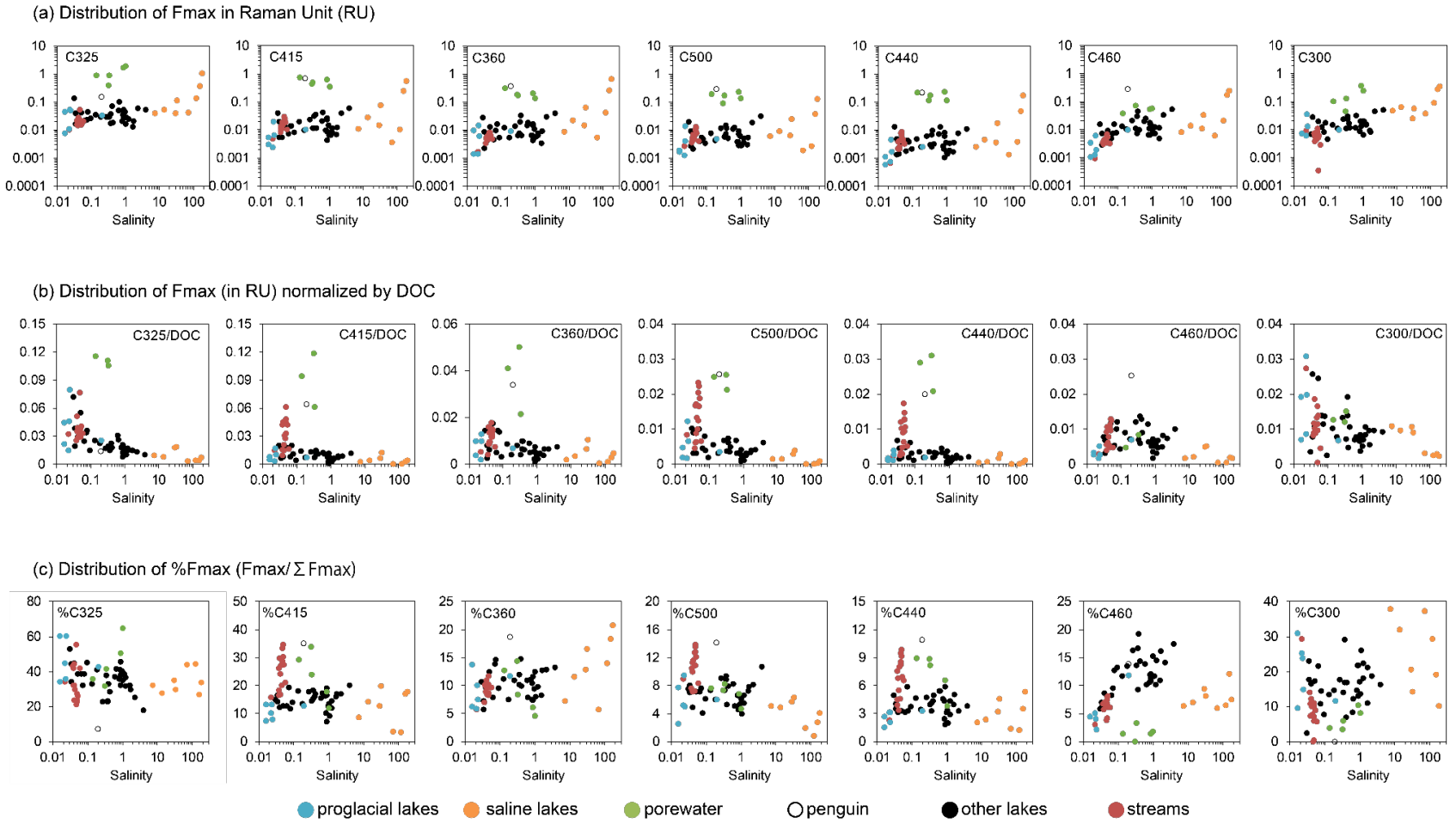


**Fig. S8.** Distribution of the identified PARAFAC components along salinity (log scale). See Fig. S6 for the sample color code interpretation.

Figure S9: Fmax/DOC of the identified PARAFAC components

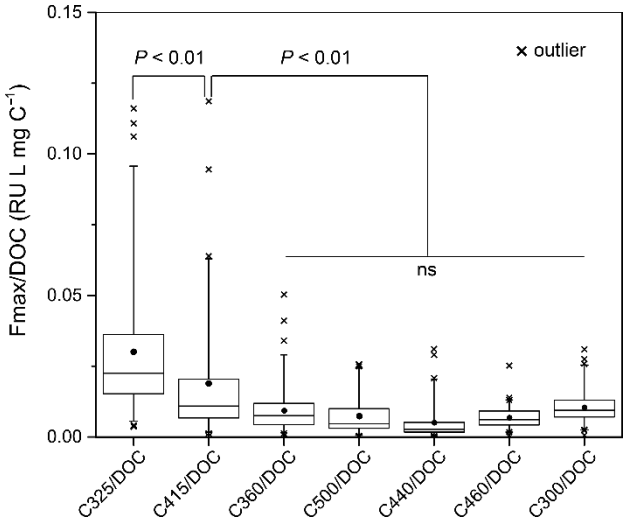


**Fig. S9.** Box plot showing the distribution of Fmax/DOC of the identified PARAFAC components. The black solid circle and line represent the mean and median, respectively. The horizontal edges of the boxes denote the 25$^{th}$ and 75$^{th}$ percentiles, and the whiskers denote the 5$^{th}$ and 95$^{th}$ percentiles.

## Table S4. Evaluation of salinity effects on CDOM and FDOM properties

Since our sample dataset encompassed large salinity differences ($S$ = 0–179), the observed differences in the optical properties may have been in part caused by the differences in salinity rather than DOM compositions between lakes. Thus, we evaluated salinity effects by changing the salinity of the solution containing the International Humic Substances Society (IHSS)'s reference sample Pony Lake fulvic acid (PLFA) at a constant pH of 8. Results showed that salinity effects are negligible on both CDOM ($S_{275–295}$; < 3%) and FDOM indices (FI, BIX, and HIX; < 0.5%) (Table S4) that showed large variations along salinity in this study (Figs. 1 and S6). Prior research has shown that increases in the ionic strength increased the absorbance (mainly 300–500 nm) and decreased a spectral slope ($S_{350–400}$) of reference DOM samples (Suwannee River humic and fulvic acids and PLFA) (Gao et al., 2015). However, the increase in the absorbance of PLFA was approximately one order of magnitude lower than that of the Suwannee River samples, and the influence of ionic strength variation was best explained with the changes of the protonation of the phenolic groups in the studied DOM (Gao et al., 2015). The non-sensitivity of PLFA to changes in salinity is consistent with the findings of Gao et al., and this indicates that effects of salinity were not quantifiable when comparing different salinity samples of predominantly autochthonous origin, and compositional change, rather than salinity, was the primary driver for variability in CDOM and FDOM properties. Similarly, the slight differences in pH (~2 unit) did not likely systematically influence our CDOM and FDOM dataset because there were no linear trends in the optical properties ($SUVA_{254}$, FI, BIX, and HIX) along pH ($P > 0.01$).

**Table S4.** Effects of salinity on CDOM and FDOM indices of Pony Lake fulvic acid (PLFA) at pH = 8. Salinity was changed by adding a desired amount of NaCl to PLFA solutions, and pH was adjusted by adding a small amount of NaOH or HCl solutions. Optical measurements were conducted after the 6-h equilibrium period.

| | Optical index | | | | Change in index values compared to $S$ = 0.188 in percentage (%) | | | |
|---|---|---|---|---|---|---|---|---|
| Salinity | $S_{275–295}$ | FI | HIX | BIX | $S_{275–295}$ | FI | HIX | BIX |
| 0.188 | 0.01436 | 1.638 | 0.8642 | 0.7722 | - | - | - | - |
| 0.452 | 0.01429 | 1.637 | 0.8657 | 0.7722 | 0.53 | 0.07 | 0.17 | 0.01 |
| 2.65 | 0.01434 | 1.635 | 0.8647 | 0.7743 | 0.15 | 0.17 | 0.06 | 0.27 |
| 25.0 | 0.01415 | 1.633 | 0.8683 | 0.7751 | 1.51 | 0.28 | 0.48 | 0.38 |
| 126 | 0.01396 | 1.630 | 0.8674 | 0.7752 | 2.82 | 0.47 | 0.36 | 0.39 |

Figure S10: Fluorescence-based indices versus $S_{275–295}$

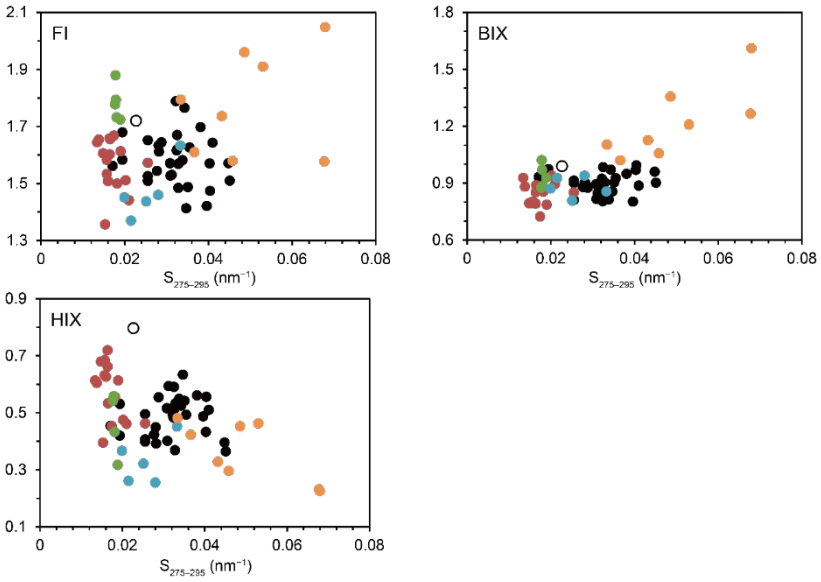


**Fig. S10.** Distribution of fluorescence index (FI), biological index (BIX), and humification index (HIX) along the spectral slope ($S_{275–295}$). Color code according to Fig S6.

The fluorescence-based indices failed to adequately capture the changes in FDOM compositions as EEM-PARAFAC did. The fluorescence index (FI) did not show any trend along $S_{275–295}$, suggesting that the DOM compositional changes, neither photodegradation nor salinity, were responsible for the large variability in FI values (1.36–2.05, Figs. S6 and S10). There was a weak positive correlation between FI and $\%C_{360}$ ($R = 0.49$, $P < 0.001$), but FI did not show the highest values in nutrient-rich saline lakes, implying that FI did not capture recent in-situ production as $\%C_{360}$ did (Fig. 3b). The large variability in FI values of autochthonous DOM complicates its use as an indicator for DOM origin. The biological index (BIX)-$S_{275–295}$ plot showed a very similar distribution pattern as the BIX-salinity plot (Figs. S6 and S10). BIX was not sensitive in capturing the changes in FDOM compositions in water types other than saline lakes, and the higher values observed for saline lakes in Fig. S6 could be due to photodegradation (Fig. S10), and not due to a change in DOM origin. Thus, a frequently observed increasing BIX values during estuarine mixing, which has been interpreted as changes in DOM origins from terrestrial to recent in-situ production (Huguet et al., 2009), should be evaluated carefully. Murphy et al. (2018) also reported up to 37% increase in BIX values after photodegradation of DOM isolates. The humification index (HIX) showed an unclear trend along $S_{275–295}$ (Fig. S10). HIX in this study had the very strong correlation with %C(ubiquitous humic + $C_{460}$) ($R^2 = 0.97$, $P < 0.001$), meaning that HIX could not resolve distinct fluorophores ubiquitous humic-like components ($C_{415}$, $C_{500}$, and $C_{440}$) and $C_{460}$, which showed very different distribution patterns along $S_{275–295}$ (Figs. 4c and 4d).

# References


Brym, A., Paerl, H.W., Montgomery, M.T., Handsel, L.T., Ziervogel, K., Osburn, C.L., 2014. Optical and chemical characterization of base-extracted particulate organic matter in coastal marine environments. Mar. Chem. 162, 96–113. doi:10.1016/j.marchem.2014.03.006

Catalá, T.S., Reche, I., Fuentes-Lema, A., Romera-Castillo, C., Nieto-Cid, M., Ortega-Retuerta, E., Calvo, E., Álvarez, M., Marrasé, C., Stedmon, C.A., Álvarez-Salgado, X.A., 2015. Turnover time of fluorescent dissolved organic matter in the dark global ocean. Nat. Commun. 6, 5986. doi:10.1038/ncomms6986

Cawley, K.M., Butler, K.D., Aiken, G.R., Larsen, L.G., Huntington, T.G., McKnight, D.M., 2012. Identifying fluorescent pulp mill effluent in the Gulf of Maine and its watershed. Mar. Pollut. Bull. 64, 1678–1687. doi:10.1016/j.marpolbul.2012.05.040

Cawley, K.M., McKnight, D.M., Miller, P., Cory, R., Fimmen, R.L., Guerard, J., Dieser, M., Jaros, C., Chin, Y.-P., Foreman, C., 2013. Characterization of fulvic acid fractions of dissolved organic matter during ice-out in a hyper-eutrophic, coastal pond in Antarctica. Environ. Res. Lett. 8, 1–10. doi:10.1088/1748-9326/8/4/045015

Cory, R.M., McKnight, D.M., 2005. Fluorescence spectroscopy reveals ubiquitous presence of oxidized and reduced quinones in dissolved organic matter. Environ. Sci. Technol. 39, 8142–8149. doi:10.1021/es0506962

Cory, R.M., Miller, M.P., McKnight, D.M., Guerard, J.J., Miller, P.L., 2010. Effect of instrument-specific response on the analysis of fulvic acid fluorescence spectra. Limnol. Oceanogr. Methods 8, 67–78. doi:10.4319/lom.2010.8.67

Farzadnia, S., Nimmagadda, R.D., McRae, C., 2017. A comparative structural study of nitrogen-rich fulvic acids from various Antarctic lakes. Environ. Chem. 14, 502. doi:10.1071/EN17095

Fichot, G., Benner, R., 2012. The spectral slope coefficient of chromophoric dissolved organic matter ( S 275 – 295 ) as a tracer of terrigenous dissolved organic carbon in river-influenced ocean margins 57, 1453–1466. doi:10.4319/lo.2012.57.5.1453

Gao, Y., Yan, M., Korshin, G. V., 2015. Effects of ionic strength on the chromophores of dissolved organic matter. Environ. Sci. Technol. 49, 5905–5912. doi:10.1021/acs.est.5b00601

Heibati, M., Stedmon, C.A., Stenroth, K., Rauch, S., Toljander, J., Säve-Söderbergh, M., Murphy, K.R., 2017. Assessment of drinking water quality at the tap using fluorescence spectroscopy. Water Res. 125, 1–10. doi:10.1016/j.watres.2017.08.020

Helms, J.R., Stubbins, A., Ritchie, J.D., Minor, E.C., Kieber, D.J., Mopper, K., 2008. Absorption spectral slopes and slope ratios as indicators of molecular weight, source, and photobleaching of chromophoric dissolved organic matter. Limnol. Oceanogr. 53, 955–969. doi:10.4319/lo.2008.53.3.0955

Huguet, A., Vacher, L., Relexans, S., Saubusse, S., Froidefond, J.M., Parlanti, E., 2009. Properties of fluorescent dissolved organic matter in the Gironde Estuary. Org. Geochem. 40, 706–719. doi:10.1016/j.orggeochem.2009.03.002

Kida, M., Fujitake, N., Suchewaboripont, V., Poungparn, S., Tomotsune, M., Kondo, M., Yoshitake, S., Iimura, Y., Kinjo, K., Maknual, C., Ohtsuka, T., 2018. Contribution of humic substances to dissolved organic matter optical properties and iron mobilization. Aquat. Sci. 80, 26. doi:10.1007/s00027-018-0578-z

Li, P., Lee, Sang Hee, Lee, Soo Hyung, Lee, J.-B., Lee, Y.K., Shin, H.-S., Hur, J., 2016. Seasonal and storm-driven changes in chemical composition of dissolved organic matter: a case study of a reservoir and its forested tributaries. Environ. Sci. Pollut. Res. 23, 24834–24845. doi:10.1007/s11356-016-7720-z

Lorenzo-Seva, U., ten Berge, J.M.F., 2006. Tucker's congruence coefficient as a meaningful index of factor similarity. Methodology 2, 57–64. doi:10.1027/1614-2241.2.2.57

Murphy, K.R., Hambly, A., Singh, S., Henderson, R.K., Baker, A., Stuetz, R., Khan, S.J., 2011. Organic matter fluorescence in municipal water recycling schemes: Toward a unified PARAFAC model. Environ. Sci. Technol. 45, 2909–2916. doi:10.1021/es103015e

Murphy, K.R., Stedmon, C. a., Graeber, D., Bro, R., 2013. Fluorescence spectroscopy and multi-way techniques. PARAFAC. Anal. Methods 5, 6557. doi:10.1039/c3ay41160e

Murphy, K.R., Stedmon, C.A., Waite, T.D., Ruiz, G.M., 2008. Distinguishing between terrestrial and autochthonous organic matter sources in marine environments using fluorescence spectroscopy. Mar. Chem. 108, 40–58. doi:10.1016/j.marchem.2007.10.003

Murphy, K.R., Stedmon, C.A., Wenig, P., Bro, R., 2014. OpenFluor- an online spectral library of auto-fluorescence by organic compounds in the environment. Anal. Methods 6, 658–661. doi:10.1039/c3ay41935e

Murphy, K.R., Timko, S.A., Gonsior, M., Powers, L.C., Wünsch, U.J., Stedmon, C.A., 2018. Photochemistry illuminates ubiquitous organic matter fluorescence spectra. Environ. Sci. Technol. 52, 11243–11250. doi:10.1021/acs.est.8b02648

Ohno, T., 2002. Fluorescence inner-filtering correction for determining the humification index of dissolved organic matter. Environ. Sci. Technol. 36, 742–746. doi:10.1021/es0155276

Osburn, C.L., Stedmon, C.A., 2011. Linking the chemical and optical properties of dissolved organic matter in the Baltic–North Sea transition zone to differentiate three allochthonous inputs. Mar. Chem. 126, 281–294. doi:10.1016/j.marchem.2011.06.007

Stedmon, C., Markager, S., 2005a. Resolving the variability in dissolved organic matter fluorescence in a temperate estuary and its catchment using PARAFAC analysis. Limnol. Oceanogr. 50, 686–697. doi:10.4319/lo.2005.50.2.0686

Stedmon, C., Markager, S., 2005b. Tracing the production and degradation of autochthonous fractions of

dissolved organic matter by fluorescence analysis. Limnol. Oceanogr. 50, 1415–1426. doi:10.4319/lo.2005.50.5.1415

Stedmon, C.A., Markager, S., Bro, R., 2003. Tracing dissolved organic matter in aquatic environments using a new approach to fluorescence spectroscopy. Mar. Chem. 82, 239–254. doi:10.1016/S0304-4203(03)00072-0

Stedmon, C.A., Thomas, D.N., Granskog, M., Kaartokallio, H., Papadimitriou, S., Kuosa, H., 2007. Characteristics of Dissolved Organic Matter in Baltic Coastal Sea Ice: Allochthonous or Autochthonous Origins? Environ. Sci. Technol. 41, 7273–7279. doi:10.1021/es071210f

Walker, S.A., Amon, R.M.W., Stedmon, C., Duan, S., Louchouarn, P., 2009. The use of PARAFAC modeling to trace terrestrial dissolved organic matter and fingerprint water masses in coastal Canadian Arctic surface waters. J. Geophys. Res. 114, G00F06. doi:10.1029/2009JG000990

Walker, S.A., Amon, R.M.W., Stedmon, C.A., 2013. Variations in high-latitude riverine fluorescent dissolved organic matter: A comparison of large Arctic rivers. J. Geophys. Res. Biogeosciences 118, 1689–1702. doi:10.1002/2013JG002320

Weishaar, J.L., Aiken, G.R., Bergamaschi, B.A., Fram, M.S., Fujii, R., Mopper, K., 2003. Evaluation of specific ultraviolet absorbance as an indicator of the chemical composition and reactivity of dissolved organic carbon. Environ. Sci. Technol. 37, 4702–4708. doi:10.1021/es030360x

Wünsch, U.J., Murphy, K.R., Stedmon, C.A., 2017. The one-sample PARAFAC approach reveals molecular size distributions of fluorescent components in dissolved organic matter. Environ. Sci. Technol. 51, 11900–11908. doi:10.1021/acs.est.7b03260

Yamashita, Y., Maie, N., Briceño, H., Jaffé, R., 2010a. Optical characterization of dissolved organic matter in tropical rivers of the Guayana Shield, Venezuela. J. Geophys. Res. 115, G00F10. doi:10.1029/2009JG000987

Yamashita, Y., Panton, A., Mahaffey, C., Jaffé, R., 2011. Assessing the spatial and temporal variability of dissolved organic matter in Liverpool Bay using excitation–emission matrix fluorescence and parallel factor analysis. Ocean Dyn. 61, 569–579. doi:10.1007/s10236-010-0365-4

Yamashita, Y., Scinto, L.J., Maie, N., Jaffé, R., 2010b. Dissolved organic matter characteristics across a subtropical wetland's landscape: Application of optical properties in the assessment of environmental dynamics. Ecosystems 13, 1006–1019. doi:10.1007/s10021-010-9370-1